Assessing mantle versus crustal sources for non-volcanic degassing along fault zones in the actively extending southern Apennines mountain belt (Italy)

Alessandra Ascione[1,†], Giancarlo Ciotoli[2,3], Sabina Bigi[4], Jamie Buscher[5,6], Stefano Mazzoli[1], Livio Ruggiero[4], Alessandra Sciarra[3], Maria Chiara Tartarello[4], and Ettore Valente[1]

[1]*Department of Earth, Environmental and Resources Science (DiSTAR), University of Naples "Federico II," 80126 Naples, Italy*
[2]*National Research Council of Italy, Institute of Environmental Geology and Geoengineering (IGAG), 00015 Monterotondo, Rome, Italy*
[3]*Istituto Nazionale di Geofisica e Vulcanologia (INGV), 00143 Rome, Italy*
[4]*Department of Earth Sciences, University of Rome Sapienza, 00185 Rome, Italy*
[5]*Andean Geothermal Center of Excellence (CEGA), Universidad de Chile, 8370450 Santiago, Chile*
[6]*Department of Geology, Facultad de Ciencias Físicas y Matemáticas, Universidad de Chile 8370450 Santiago, Chile*

ABSTRACT

The actively extending axial zone of the southern Apennine mountain belt of Italy is characterized by a substantial flow of non-volcanic gas to the surface. In this study, we have analyzed the correlation between the active tectonic framework of the Matese Ridge area and the high gas emissions found to the southwest, which includes large amounts of CO_2 (up to 99 vol%), CH_4 (up to 0.55 vol%), and He (up to 52 ppmv). We measured CO_2 and CH_4 fluxes of up to 34000 g d^{-1} and 2000 g d^{-1}, respectively, from zones of focused degassing (gas vents and associated strong diffuse emission). This anomalously high flux of CO_2 (advective plus diffusive) indicates that the study area has one of the largest non-volcanic natural emissions of CO_2 ever measured on Earth. The isotope composition of C in CO_2 and CH_4 shows there is a dominant crustal contribution of emissions (as opposed to a source from the mantle), indicating that thermometamorphism of the buried Apulian Platform carbonates is probably the main cause of CO_2 production. This process has likely been enhanced by Quaternary magmatism, which provides an additional local source of heat triggering decarbonation of Apulian Platform limestones and dolostones at depth. The advective flux is concentrated at gas vents located along active fault segments located at the western tip of a major crustal structure, the South Matese fault zone. We believe that the very high gas emission in the Matese Ridge area is the result of both the presence of a dense network of active fault strands, which provides efficient pathways for fluid flow toward the surface, and the dramatically reduced thickness of the clay-rich mélange zone acting elsewhere in the southern Apennines as a top seal overlying the buried Apulian Platform carbonates.

INTRODUCTION

Natural degassing of massive amounts of CO_2 occurs along the entire Apennines mountain belt of Italy (Chiodini et al., 2004; Minissale, 2004; Frezzotti et al., 2009; Burton et al., 2013). Very high fluxes of geogenic CO_2 (up to $1–2 \times 10^{11}$ mol y^{-1}; Chiodini et al., 2013) are measured along the southwestern part of the Apennines, particularly in the central-southern segment of the Tyrrhenian back-arc basin margin, where there is evidence for Quaternary and active volcanism. In this area, the presence of thinned crust and mature sets of extensional faults and fracture systems allows crustal and/or mantle fluids feeding the volcanic systems to migrate toward the surface (Chiodini et al., 1999, 2000, 2004, 2013; Chiodini and Frondini, 2001; Mörner and Etiope, 2002; Gambardella et al., 2004; Burton et al., 2013; Etiope, 2015).
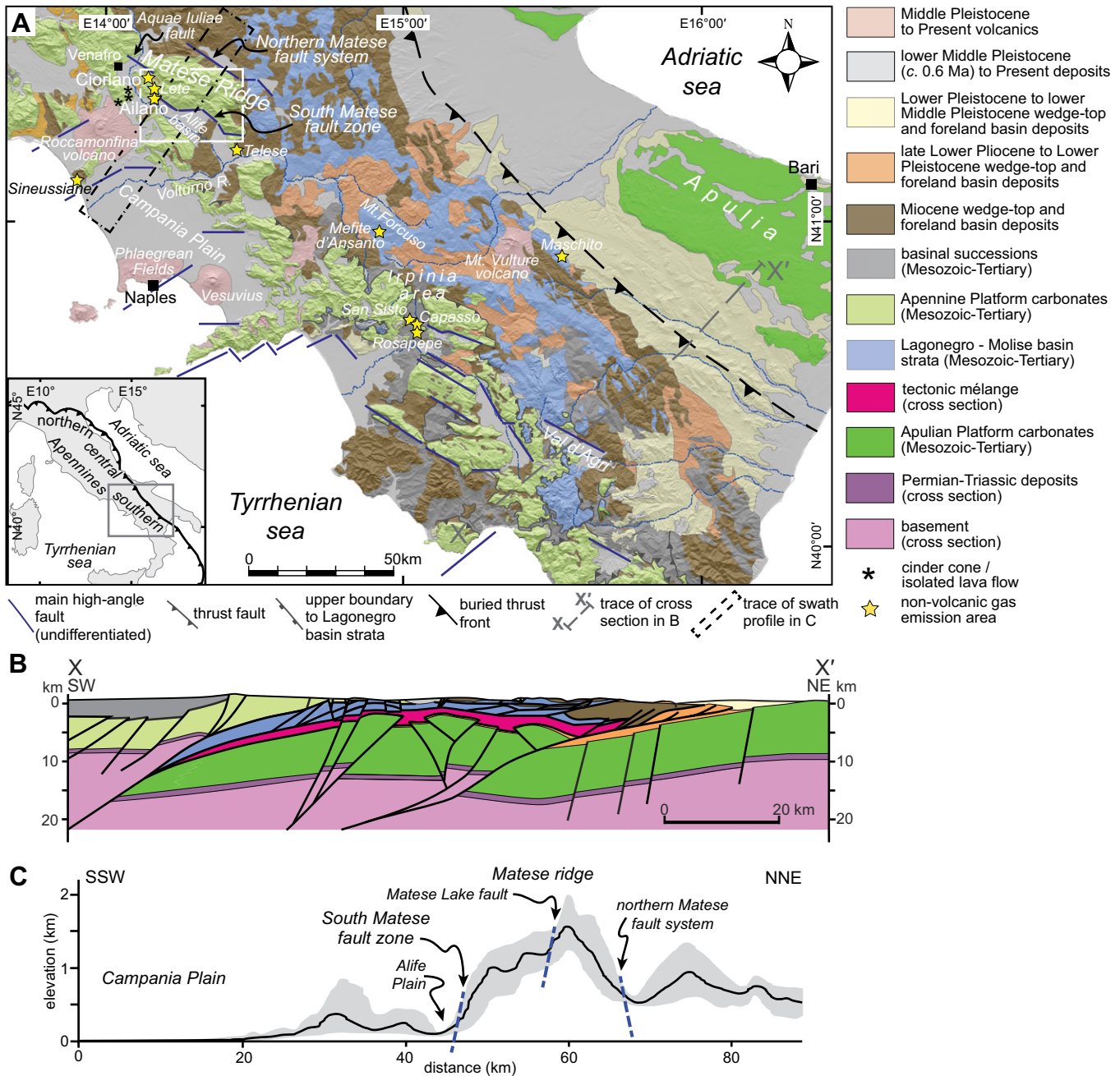
Natural CO_2-dominant gas manifestations also occur in areas of the Apennines not affected by volcanic activity (i.e., non-volcanic areas). The isotopic signature (i.e., ^{13}C and ^{3}He/^{4}He) of the majority of non-volcanic gas emissions suggests that the gas is primarily produced by a combination of upper mantle degassing and/or metamorphic decarbonation of marine limestones (Chiodini et al., 1999, 2004; Italiano et al., 2000, 2008; Minissale, 2004; Caracausi et al., 2013). Current models of degassing in non-volcanic areas of the Apennines imply that the process occurs from a deep hot source ("mantle wedge") and by the progressive dehydration of the subducted Adriatic-Apulian plate (Chiodini et al., 2004, 2013; Frezzotti et al., 2009; Chiarabba and Chiodini, 2013). Also, mechanical energy released during seismic events has been recently proposed as a possible additional source of CO_2 (through friction-related heating and associated decarbonation processes; e.g., De Paola et al., 2011) for areas in the Apennines where the contribution of CO_2 degassing from the mantle is low (Italiano et al., 2008).

Non-volcanic gas emissions are mostly localized within Quaternary continental grabens that punctuate areas along the axis of the central and southern Apennines mountain belt. This axial region is currently affected by extensional processes, which control the moderate to strong seismicity that affects the Italian peninsula (e.g., Rovida et al., 2016). Additionally, there is evidence for both CO_2 and CH_4 emissions occurring at the surface along active fault systems (Chiodini et al., 2004; Ciotoli et al., 2007; Ciotoli et al., 2014; Caracausi and Paternoster, 2015).

In the southern Apennines, CO_2 emissions are widespread, but we have focused this study on the high gas emissions occurring in areas surrounding the Ciorlano and Ailano villages located southwest of Matese Ridge (Fig. 1). In the Ailano area, we have identified a very high density of gas vents (~200 in ~2 km^2) that to date

Figure 1. (A) Geological map of the southern Apennines (modified from Ascione et al., 2013) indicating the main non-volcanic gas emission areas. (B) Geological cross section of the southern Apennines (after Mazzoli et al., 2014). (C) Topographic swath profile (10 km in width) of the southern Apennines spanning across the Matese area. The white box in diagram A indicates the location of the study area, shown in Figure 3.

represents a unique location for gas emissions relative to other areas in Italy.

In the Matese Ridge area, we have carried out a multidisciplinary study aimed at characterizing the spatial relationship between the active fault framework and the network of gas emissions. First, we carried out a tectonic geomorphology investigation to search for indicators of late Quaternary tectonic activity in the region, including the southern mountain front of Matese Ridge and the topographic lows to the west where no strong historical earthquake has been localized. Second, we conducted extensive and detailed-scale soil gas and gas flux surveys to examine the chemical composition of the gases emitted from both vents and diffuse emissions, and preliminarily quantified the total geogenic CO_2 from the investigated area. In addition, we analyzed isotope $\delta^{13}C$ in CO_2 and CH_4, and the He isotopic ratio ($^3He/^4He$) to constrain the gas source at depth.

Based on the inferred gas source from the isotope analyses, the spatial distribution of the continuous leakage and diffuse degassing, and the reconstruction of the active tectonics framework, we propose a new interpretation for the generation and complex migration of fluids through the southern Apennines thrust belt.

TECTONIC FRAMEWORK

The southern Apennines are part of the Alpine-Apennine orogenic system, which formed from convergence of the African and Eurasian plates from the Late Cretaceous to the Quaternary (e.g., Mazzoli and Helman, 1994; Turco et al., 2012, and references therein). From the Neogene to Early Pleistocene, thrusting was coeval with back-arc extension and the opening of the Tyrrhenian Sea (e.g., Butler et al., 2004, and references therein). Since the Early Pleistocene, extensional processes have produced large coastal grabens (e.g., Savelli and Schreider, 1991; Sartori, 2003) punctuated by intense magmatic activity along the Tyrrhenian margin of the southern Apennines. Starting at ca. 0.4 Ma, strong explosive volcanic activity occurred at several eruptive centers located within the Campania Plain graben and at the Roccamonfina volcano (e.g., Luhr and Giannetti 1987; De Rita et al., 1998; Brocchini et al., 2001; Rolandi et al., 2003; Rouchon et al., 2008; Fig. 1A). In the Middle Pleistocene, there was also emplacement of peripheral dikes and eccentric monogenetic volcanoes in the region west of Matese Ridge (Di Girolamo et al., 1991; Fig. 1A). In the Matese area, the presence of a magmatic reservoir at a depth of ~10 km has been inferred from the occurrence of a 2–3-km-thick low S-wave velocity (Vs) layer (Nunziata and Gerecitano, 2012).

During the Middle Pleistocene, magmatism occurred also in the frontal part of the thrust belt at the Vulture volcano (Principe, 2006; Fig. 1A). Magma rising in this area was most likely associated with the development of a lithospheric tear in the subducting slab (e.g., De Astis et al., 2006; D'Orazio et al., 2007; Ascione et al., 2012).

The southern Apennines accretionary wedge is composed of both ocean and continental margin-derived tectonic units (Ciarcia et al., 2012; Vitale et al., 2013; Fig. 1). The latter units were formed by Mesozoic–Tertiary carbonate platform/slope successions (related to the Apennine Platform) and pelagic basin (Lagonegro–Molise Basin) successions, and are stratigraphically overlain by Neogene foredeep and wedge-top basin sediments (e.g., Ascione et al., 2012; Mazzoli et al., 2012). At the surface are low-angle tectonic contacts that separate the Apennine Platform carbonates in the hanging wall from the Lagonegro Basin successions in the footwall (Mazzoli et al., 2008). These tectonic contacts consist of both thrusts, in part reactivated during extensional stages, and newly formed low-angle normal faults (Mazzoli et al., 2014). The Apennine accretionary wedge is thrusted onto the Apulian Platform, which has a thickness of 6–8 km and consists of a Mesozoic–Tertiary shallow-water carbonate succession that is ex-posed in the foreland to the northeast (Shiner et al., 2004, and references therein; Fig. 1B). The contact between the allochthonous units and the buried Apulian Platform unit is marked by a fluid-saturated, clay-rich mélange zone of variable thickness, reaching ~1500 m in the Val d'Agri area (Mazzoli et al., 2001; Fig. 1B). Such a mélange zone acts as a seal for fluids escaping the Apulian Platform in this region, which hosts Europe's largest onshore oil fields (Shiner et al., 2004). In the Irpinia area to the north (Fig. 1A), a high P-wave to S-wave velocity ratio (V_P/V_S) recorded by seismic tomography points to the presence of fluid reservoirs below the mélange zone (Amoroso et al., 2014), consisting of brine-CO_2/CH_4 or CO_2-CH_4 mixtures (Amoroso et al., 2017).

Based on the interpretation of the CROP-04 deep seismic reflection profile, the fluid reservoir corresponds to the lower section of the Apulian Platform and underlying Permo–Triassic clastic deposits, reaching the top of the crystalline basement (Ascione et al., 2013). Information on the stratigraphy of the lower part of the Apulian Platform is provided by two deep wells (Gargano 1 and Puglia 1, available from the Visibility of Petroleum Exploration Data in Italy-ViDEPI Project; ViDEPI, 2010), which were drilled for oil exploration in the Apulian foreland. In the Gargano 1 and Puglia 1 well logs, Lower Jurassic limestones are underlain by ~2.5 km of dolostones with thick anhydrite intercalations (Burano Formation, Middle–Upper Triassic), followed by ~1000 m of clastic rocks (sandstones, siltites, and argillites) of Permian to Lower Triassic age.

The buried Apulian Platform is characterized by reverse-fault-related, open, long-wavelength folds (Fig. 1B) that form the hydrocarbon traps for oil fields in the southern sector of the thrust belt (Shiner et al., 2004). Geophysical evidence shows that the crystalline basement is involved in deep-seated reverse faulting (Speranza and Chiappini, 2002; Improta and Corciulo, 2006; Steckler et al., 2008). The associated deformation is represented by vertical offsets along steep reverse faults, with relatively limited horizontal displacements (Shiner et al., 2004; Mazzoli et al., 2014).

In the southern Apennines, crustal shortening ceased in the Middle Pleistocene (e.g., Patacca and Scandone, 2001), when NE-SW–oriented horizontal extension became dominant over the entire orogen (e.g., Hippolyte et al., 1994). Extensional faults, mainly NW-SE–trending, post-dating and dissecting the thrust belt (e.g., Butler et al., 2004) are also responsible for the active tectonics and seismogenesis in the southern Apennines (e.g., Cello et al., 1982, 2000; Westaway, 1992; Chiarabba et al., 2005; Pondrelli et al., 2006; Maggi et al., 2009; Frepoli et al., 2011; Macchiavelli et al., 2012; Ascione et al., 2013; DISS Working Group, 2015).

Geological Setting and Historical Seismicity of the Matese Area

Matese Ridge is composed of Triassic to Cretaceous carbonates and Miocene calcarenites as part of the Apennine Platform thrust sheet, which is locally covered by late Miocene wedge-top deposits (Fig. 1A). The top surface of Matese Ridge features karst topography characterized by several internally drained basins (e.g., the Matese Lake basin; Santangelo and Santo, 1991; Aucelli et al., 2013; Valente et al., 2018), and karst gorges, such as the Torano Stream (Lambiase and Ruggiero, 1980), which sinks underground to the east of San Gregorio Matese and emerges a few hundred meters downstream.

Carbonates outcropping in Matese Ridge consist of inner platform to by-pass and slope facies successions, separated by high-angle faults that originally acted as normal faults in the Mesozoic, which were reactivated during Miocene shortening with minor reverse displacement (Calabrò et al., 2003). The Apennine Platform carbonates are thrusted northward over Mesozoic to Tertiary successions related to the Molise Basin, which crop out to the north and east of Matese Ridge and overlie the buried and deformed Apulian Platform carbonates (Butler et al., 2000, and reference therein; Calabrò et al., 2003). The thrust pile is dissected by NW-SE–trending extensional structures and E-W–trending high-angle faults that generally exhibit left-lateral offsets, which have been overprinted by faults that have either pure dip-slip or oblique-slip (with a right-lateral component) motion associated with extensional reactivation during the Middle Pleistocene to Present tectonic regime (Butler et al., 2004, and references therein). Two main extensional fault zones composed of NW-SE and E-W–striking structures bound the Matese Ridge on the northeast and southwest: the northern Matese fault system with evidence of Middle Pleistocene to Holocene activity (Galli et al., 2017), and the South Matese fault zone (SMF), respectively. These structures control the formation of Quaternary continental basins including the Alife Basin (Fig. 1A), which is filled by a Middle Pleistocene to Holocene succession that is several hundreds of meters thick (Corniello and Russo, 1990). Several of the Quaternary faults in the Matese Ridge area show evidence of late Quaternary activity (Cinque et al., 2000, and references therein), including the Aquae Iuliae fault, which dissects the western part of the ridge and reflects activity in the Holocene (Galli and Naso, 2009; Amato et al., 2017; Fig. 1).

The Matese Ridge area is located in the epicentral area of multiple strong historic earthquakes. The most destructive events, with Mercalli-Cancani Sieberg intensities of X–XI, occurred in 1349, 1456, 1688, and 1805 and created ground effects such as surface faulting, sinkholes and landslides that led to thousands of casualties (e.g., Esposito et al., 1987; Gasperini et al., 1999; Michetti et al., 2000; Galli and Galadini, 2003; Di Bucci et al., 2005; Fracassi and Valensise, 2007; Porfido et al., 2007; Serva et al., 2007; Galli and Naso, 2009; Santo et al., 2011; Locati et al., 2011; Rovida et al., 2016; Fig. 2). The 1688 and 1805 earthquakes were related to NW-SE–oriented, NE-dipping seismogenic sources, located at the northeastern and northern boundaries of the Matese Ridge, respectively (Boschi et al., 1997; DISS Working Group, 2015), while the 1349 earthquake was related to the SW-dipping Aquae Iuliae fault (Galli and Naso, 2009). Since 1805, the Matese area has been affected by background seismicity with an infrequent number of earthquakes and seismic sequences (Alessio et al., 1990; Milano et al., 1999, 2002, 2005, 2006; Valensise and Pantosti, 2001; Fig. 2). On 29 December 2013, a moment magnitude (Mw) = 5.16 ± 0.07 earthquake oc-

curred (Rovida et al., 2016), which was located in the southeastern part of Matese Ridge (http://cnt.rm.ingv.it/tdmt.html; Fig. 2). This earthquake was characterized by a normal fault mechanism with a NE-oriented T axis, which caused a series of coseismic surface effects including landslides and ground ruptures (Valente et al., 2018).

To the south of Matese Ridge, several areas have surface gas emissions (surroundings of Ciorlano and Ailano; e.g., Googas, 2006; Fig. 1A), and/or a variety of surface phenomena that may be associated with the localized rising of fluids. Such phenomena include: (*i*) mineral springs (e.g., Acqua Lete mineral water springs; Corniello et al., 1999) in the Pratella area; (*ii*) thermal springs in the Telese and Venafro areas, with the chemical composition of the Telese springs reflecting deep-seated sources (Italiano et al., 2000); (*iii*) calcareous tufa and travertine deposits (surroundings of Venafro and Telese), with the $\delta^{13}C$ isotope composition of carbonates bearing a crustal signature (Ascione et al., 2014); and (*iv*) clusters of sinkholes formed in carbonate rocks (around Pratella and Telese), which are related to enhanced dissolution associated with fluids rising along active faults (Santo et al., 2011).

MATERIALS AND METHODS

Tectonic Geomorphology Analysis

A wide-ranging tectonic geomorphology analysis aimed at reconstructing the Quaternary tectonics framework of the southern Matese Ridge and adjoining basins was carried out through a combination of field surveys and topographic analyses of both digital elevation models (DEM) and detailed-scale topographic maps. Details of the different approaches utilized in this study are outlined below.

The chronological framework for fault activity was based on cross-cutting relationships between the faults and Quaternary units of different relative ages and a variety of geomorphological indicators.

Stratigraphic Analysis of Quaternary Units

Information on stratigraphy, thickness and features of alluvial units both outcropping and buried was obtained by field surveys and inferred from the interpretation of 102 published and unpublished shallow borehole logs drilled from hilly to flat-lying areas surrounding Matese Ridge and having depths ranging from 8 to 309 m. Most of the Quaternary alluvial units (both outcropping and buried) are interlayered with tephra layers up to several m thick and include the distinctive ≥10-m-thick, 40 ka (De Vivo et al., 2001) Campanian Ignimbrite regional chronostratigraphic marker. This marker unit outcrops regularly in the investigated area (e.g., Servizio Geologico d'Italia, 1966), and has been identified in the logs. These pyroclastic layers generally provide a lower age limit for correlative alluvial units, which based on the ca. 400 ka age of initiation of explosive activity from volcanic centers in the study region (e.g., Brocchini et al., 2001; Rolandi et al., 2003; Rouchon et al., 2008), may be related to the upper part of the Middle Pleistocene or a younger time period. Relative chronology of the continental units was inferred from geomorphological-stratigraphical criteria, which includes the height above local base level of terraces, vertical separation between inset terraced units, degree of incision of terraces/alluvial fans and morpho-stratigraphical relationships with the Campanian Ignimbrite marker unit.

Geomorphological Analysis

A detailed-scale geomorphological analysis of the entire study area was carried out by field surveys and analysis of 1:5000 topographic maps published by the Regione Campania. Late Quaternary fault activity was inferred by classical geomorphological indicators, including fault scarps formed in alluvial deposits, relic stream
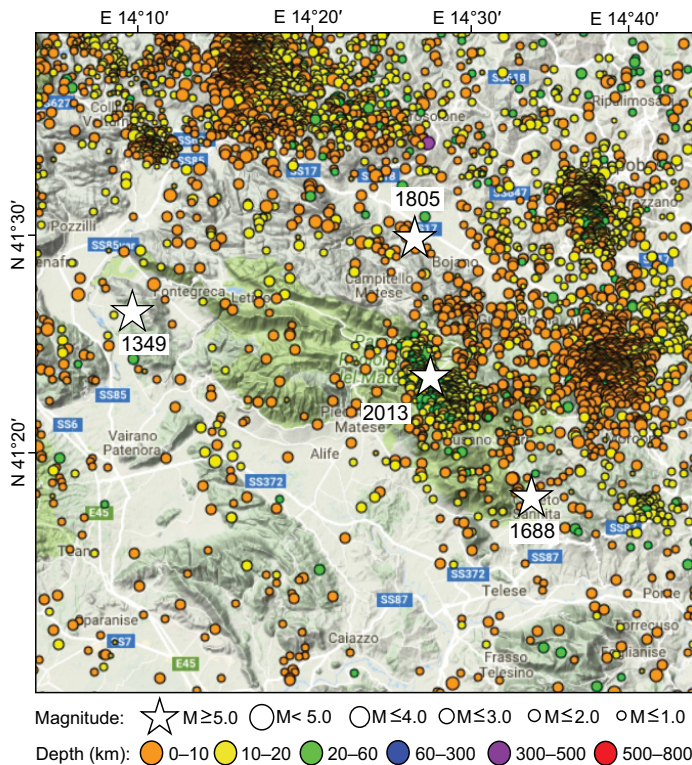
Figure 2. Seismicity recorded from 1990 to the Present (derived from the ISIDe database; http://iside.rm.ingv.it/iside) and locations of epicenters of strong historical earthquakes in the Matese Ridge region, derived from Galli and Naso (2009) and the Parametric Catalogue of Italian Earthquakes 2015 (Rovida et al. 2016).

features (e.g., wind gaps and beheaded valleys, etc.), and active drainage network features, such as the alternation of embayment reaches/localized depocenters with wind gaps/water gaps along river valleys and anomalous flow orientations and/or bends of streams that dissect Quaternary surfaces formed in alluvium (e.g., terraces, alluvial fans, alluvial plains).

Since steep carbonate escarpments in the Apennines are not always indicative of recent surface displacements (escarpments may form from either differential erosion of old—Miocene to Pliocene—fault planes, or early and/or late Quaternary offsets (e.g., Ascione and Cinque, 1999; Ascione et al., 2013), particular attention was placed on the geomorphological analysis of the southern mountain front of Matese Ridge. The analysis focused on the construction of a swath profile transverse to Matese Ridge using a 90 m DEM (NASA Shuttle Radar Topography Mission) and a detailed-scale map study devoted to the detection of indicators of recent—i.e., late Quaternary—fault displacements. The detailed-scale study included a comparison of past and present-day positions of hydrographic apexes of alluvial fans relative to the mountain front to provide insight on the variation of accommodation space in the hanging wall of extensional faults (e.g., Bull, 2008).

The topographic analysis was also focused on the identification and mapping of sinkholes formed in alluvium (deep piping sinkholes sensu Caramanna et al., 2008) and in carbonate rocks (karst collapse sinkholes sensu Santo et al., 2011).

Stream Profile Analysis

To provide insight on the topographic response to uplift in the core of the Matese Ridge and surrounding areas, major trunk and tributary streams were analyzed using a 10 m DEM base map created by the interpolation of contour lines derived from 1:5000 topographic maps published by the Regione Campania. Thirty-four profiles extending from stream headwaters to mountain outlets were extracted from the 10 m DEM and analyzed. The streams were distinguished between graded profiles with concave-upward curvatures typical of mature mountain belts (e.g., Hack, 1957) and streams with exceptionally convex-upward profiles that may represent regional surface uplift or a transient response to an increased fault uplift rate on a local scale (e.g., Kirby and Whipple, 2001; Whittaker et al., 2007; Attal et al., 2011). In particular, a comparison of the magnitude of convexities may reveal a variable slip rate along the same fault segment or between faults (Whittaker et al., 2008; Ascione et al., 2013). To quantify the degree of profile convex-

ity, the raw stream profiles were plotted (using the stream profile tool of Whipple et al. (2007) [http://geomorphtools.geology.isu.edu/Tools/StPro/StPro.htm]) and compared with two reference profiles: (a) a concave-up stream profile reflective of a typical graded stream based on the natural log curve between the upstream and downstream end points of the stream, and (b) a rectilinear line between the same two points representative of a surface where uplift exceeds fluvial downcutting (Buscher et al., 2017). Streams for the convexity analysis extended from headwaters to the mountain front because comparison of stream profiles is based on bedrock-floored streams and any extension of the profile into the alluvial fan area would deviate from this line of reference.

Soil Gas Sampling and Analysis

A soil-gas and flux measurement survey was performed in two areas located to the west of Matese Ridge, i.e., the Ailano and Ciorlano sites, in July 2015 during a period of stable meteorological conditions (i.e., an average day temperature of 25 °C and no precipitation). A total of 575 soil gas samples were collected at the two sites with a sampling density of ~400 sample/km^2 and 200 sample/km^2 at the Ciorlano (229 samples) and Ailano (346 samples) sites, respectively. Field analyses were conducted for carbon dioxide (CO_2, range 0%–100%), oxygen (O_2, range 0%–21%), hydrogen (H_2, range 0–600 ppm), and hydrogen sulfide (H_2S, range 0–1000 ppm) (accuracy <5%) by directly attaching a 6.4 mm, thick-walled, stainless-steel tube in the soil at a depth of ~0.6–0.8 m to a portable gas analyzer (Multiwarn Xam-7000, Draeger Instruments) (Ciotoli et al., 2007; Beaubien et al., 2015). Field analyses were also conducted for Radon (Rn) by pumping gas directly from the probe into the Lucas cell of an RDA200 detector (EDA-Scintrex Instruments).

Complementing in situ measurements, soil gas samples were collected and stored in a previously-evacuated, 25 mL stainless-steel canister sealed with a rubber septum for laboratory analyses of major gases (O_2+Ar, N_2, CO_2) (accuracy ± 2%), and for C1–C4 alkanes (accuracy ± 3% at 2 ppmv; detection limit 0.1 ppmv) by using two Fisons 8000-series Bench gas chromatographs. Helium (He) was also analyzed for these samples using a mass spectrometer (Varian Leak Detector; 10–4 atm cc/sec to 4 × 10–8 atm cc/sec). The statistical analysis of CO_2 and O_2 between the field and laboratory measurements exhibits a linear fit with R = 0.994 and a regression fit with R^2 = 0.989 (R—linear correlation coefficient, R^2—regression coefficient).

Gas Flux Measurements

Direct measurements of 527 CO_2 flux measurements from the ground were performed both at the Ciorlano (181 measurements) and Ailano (386 measurements) study sites using a home-made static closed-chamber system (0.2 × 0.2 × 0.1 m) connected with a portable CO_2 non-dispersive infrared sensor (Gascard NG, dimensions 160 × 100 mm, Edinburgh Instruments Ltd.) (Beaubien et al., 2015). The sensor has a measurement range of 5000 ppm with a resolution of 1 ppm and an accuracy of ± 2%. It has a low operating voltage (7V) and is equipped with true RS232 communication for control and data logging, zero and span adjust and gas I/O (the gas flow is ~1.0 l/min). The gas fluxes are automatically calculated by a linear regression of the gas concentration build-up (ppmv/s) in the chamber; fluxes are expressed as g CO_2 m^{-2} d^{-1} as reported in the literature for the gas seepage and biological fluxes from soils.

Molecular and Isotopic Analysis

Gas samples for the isotopic analyses were collected at the ground surface from three visible major gas vents (using a funnel for bubbling emissions and a soil gas probe for dry emissions from the soil) and stored in 250 mL glass tubes equipped with two vacuum stop-cocks, or in 25 mL stainless-steel canisters equipped with a Swagelok valve. Samples were analyzed at Isotech Labs Inc. (Illinois, USA) for C_1–C_6 hydrocarbons, He, H_2, Ar, O_2, CO_2, N_2 (Shimadzu 2010 TCDFID GC; accuracy and precision 2% [1σ]), and stable carbon and hydrogen isotopic ratios of CH_4 and CO_2 ($\delta^{13}C_{CH_4}$, $\delta^2H_{CH_4}$, $\delta^{13}C_{CO_2}$; Finnigan Delta Plus XL mass spectrometer, precision ± 0.3‰ (1σ) for ^{13}C, ± 4‰ (1σ) for ^2H). Stable C and H isotopic ratios are referenced to the Vienna Pee Dee belemnite (VPDB) and Vienna standard mean ocean water (VSMOW) standards, respectively.

The abundance and isotope composition of He, and the $^4He/^{20}Ne$ ratios, were determined by separately admitting He and Ne into a split flight tube mass spectrometer (GVI Helix SFT mass spectrometer). The analytical errors were generally <1% (Paonita et al., 2012). The helium isotopic ratios are expressed as R/R_A, where R is the $^3He/^4He$ ratio of a sample corrected for air contamination using the measured abundance of atmospheric neon, and then this is compared to the ratio of those isotopes in air (R_A amounting to 1.386 10^{-6}) (Craig et al., 1978).

Statistical Analysis of Soil Gas Concentrations and Flux Measurements

Exploratory data analysis techniques were applied to interpret and map CO_2 soil gas concentrations and flux data in order to identify

interacting processes within the data distribution, such as anomalous values caused by advective gas migration from a deep source and diffusive gas emissions, as well as biological sources (e.g., Filzmoser et al., 2005; Reimann et al., 2005; Ciotoli et al., 2007; Etiope et al., 2011). Traditionally, the statistical evidence of interacting processes is recognized by using histograms, box-plots and scatterplots coupled with the calculation of some statistical indexes (e.g., mean, median, standard deviation, quantiles, etc.). These values constrain the upper and lower limits of the normal variation of a particular population of data (i.e., advective anomalies, diffusive processes, biological sources). Scatterplots of CO_2 vs N_2 and O_2 concentrations in soil gas were used to highlight the amount of CO_2 derived by leakage from a deep source (dilution of N_2 and O_2) and from biological respiration (Beaubien et al., 2008; Romanak et al., 2012). The normal probability plot (NPP) was used to recognize the statistical threshold values among the different populations (Sinclair, 1991).

Geospatial Analysis

The presence of both main vents (MV) and secondary vents (SV) increases the variance of CO_2 flux values throughout the study area, so it was necessary to distinguish and elaborate separately the fluxes having a difference equal to or more than three orders of magnitude (i.e., values ranging from 10^0 to 10^4 g m^{-2} d^{-1} cannot be elaborated together). At the Ciorlano site, the limited spatial extent of the investigated area and the presence of only a few MV of relatively high magnitude required that the maps of CO_2 flux and CO_2 concentrations be obtained by using the natural neighbor algorithm, which provides the best contour estimates for sampling of irregularly spaced points to avoid the overestimation of the flux outside the advective vent area and outside the study area (Sibson, 1981). In contrast, a geostatistical analysis (i.e., variogram modeling and kriging algorithm) was applied to the larger Ailano site to verify if the spatial distributions of CO_2 flux and CO_2 gas concentrations produce a pattern that follows the orientation of specific structural features (e.g., fault-related anisotropy). In particular, the presence of a high density and high magnitude MV in the Ailano area affects flux values that show very high variability (from 10^0 to 10^4 g m^{-2} d^{-1}). For a more reliable reconstruction of the estimate map, as well as for a preliminary quantification of the CO_2 flux, the data were elaborated using variogram modeling and an ordinary kriging algorithm. Helium data have been represented by overlapping dot maps onto CO_2 concentration and flux contour maps. These maps were then used to analyze possible correlations between the distribution of the MV and SV with the orientation of faults active during the late Quaternary.

Fluid Data from Deep Wells

A large amount of subsurface data—particularly seismic reflection profiles and well logs—acquired by the oil industry is available for the southern Apennines. Important subsurface constraints for this study were obtained by well log data from the ViDEPI inventory (ViDEPI Project, 2010). This inventory is a collection of all documentation relating to expired, and therefore public, mining permits and concessions, filed since 1957 with the National Mining Office for Hydrocarbons and Georesources (UNIMIG) of the Ministry for Economic Development. The data from the ViDEPI files have been examined in order to obtain information about the nature and amount of fluids encountered in the drill holes throughout the southern Apennines.

GEOMORPHOLOGICAL-STRATIGRAPHICAL CONSTRAINTS FOR THE LATE QUATERNARY FAULT ACTIVITY

The large-scale topographic features of the Matese area and surrounding region are synthesized in the swath profile of Figure 1C. In the profile, the 2050 m high Matese Ridge appears as a prominent topographic high with an overall asymmetrical shape. In fact, the profile of the southwestern slope appears steeper and slightly convex while that of the northeastern flank is less steep and slightly concave. High local-relief at the boundaries of the Matese Ridge is associated with the northern Matese fault system (Galli et al., 2017) to the NE and the South Matese Fault zone (SMF) to the SW (Fig. 3). The profile shows that the top surface of the southern part of Matese Ridge has a mean elevation range of 1000–1500 m (Fig. 1C) and is bounded to the NE by an abrupt step in the elevation curve, which may be interpreted as the surface expression of a SW-dipping fault system including the Matese Lake extensional fault that is believed to reflect late Quaternary activity (Cinque et al., 2000; Ferranti et al., 2015; Figs. 1C and 3).

Geophysical data from the Alife Basin (Corniello and Russo, 1990) show that the top of the carbonate units of Matese Ridge, located in the hanging wall block of the SMF, is downthrown to a depth of ~600 m below sea level (b.s.l.) (Fig. 3). The Alife Basin includes the flat and undissected Volturno River floodplain, which grades from ~110 m to 70 m above sea level (a.s.l.) from west to east, and the smooth Torano stream alluvial fan (Fig. 3). Alluvial deposits found at the Alife Basin surface represent

the top of an alluvial succession that, based on published (Corniello and Russo, 1990) and unpublished subsurface stratigraphy data, consists of lacustrine deposits with a thickness of at least 200 m. The deposits are mostly made up of fine-grained sediments interlayered with calcareous tufa and travertine beds up to several tens of meters thick as well as fluvial gravels that are laterally interfingered (toward the north) with coarse-grained alluvial fan deposits. Toward the south, the Volturno River alluvial plain is inset into terraces standing at ~20 m above the plain. The terrace risers, which consist of straight scarps oriented E-W and ENE-WSW (Fig. 3), expose distinctive pyroclastic deposits that are tens of meters thick, based on unpublished borehole logs. We correlate these pyroclastic deposits with the 40 ka Campanian Ignimbrite unit (De Vivo et al., 2001), which is also identified in the shallow subsurface of the Alife area beneath a several meter thick layer of Holocene lacustrine deposits (Paris and Sevink, 1983). To the east, the Alife Basin is bounded by a roughly N-S–oriented topographic high, which consists of Miocene sandstones overlain by alluvial fan deposits (Fig. 3). Moving away from this topographic high, the Volturno River joins with the Titerno River, which flanks the easternmost segment of the SFM and turns to the south toward the Campania Plain graben (Fig. 1).

The Alife Basin depocenter tends to become narrower and shallower from east to west (Fig. 3). In the west, the Volturno River alluvial plain is bounded to the north by a hilly landscape formed of Mesozoic and Tertiary rocks and Quaternary deposits that are dissected by the Lete River, a left-side tributary of the Volturno River (Fig. 3). The upper part of the Lete River hydrographic network dissects terraced alluvial units that have filled the Ciorlano Basin (Fig. 3).

The Matese Ridge Southern Mountain Front

The southern flank of Matese Ridge is characterized by a faceted mountain front of variable orientation and height, with elevation decreasing from ~1300 m in the core of the ridge to ~600 m to both the east and west. The piedmont consists of an array of coalescing alluvial fans (Santangelo et al., 2012). In the west (Ailano Hills area), the Matese Ridge escarpment maintains a NW-SE orientation, while an ~E-W–oriented scarp marks the sharp boundary between the bajada to the south and the Mesozoic carbonates to the north (Fig. 3).

A distinct ~E-W variation of the surface and alluvial fan features is observed in the piedmont. In the eastern part, alluvial fans are inactive and deeply incised by both the feeding streams and
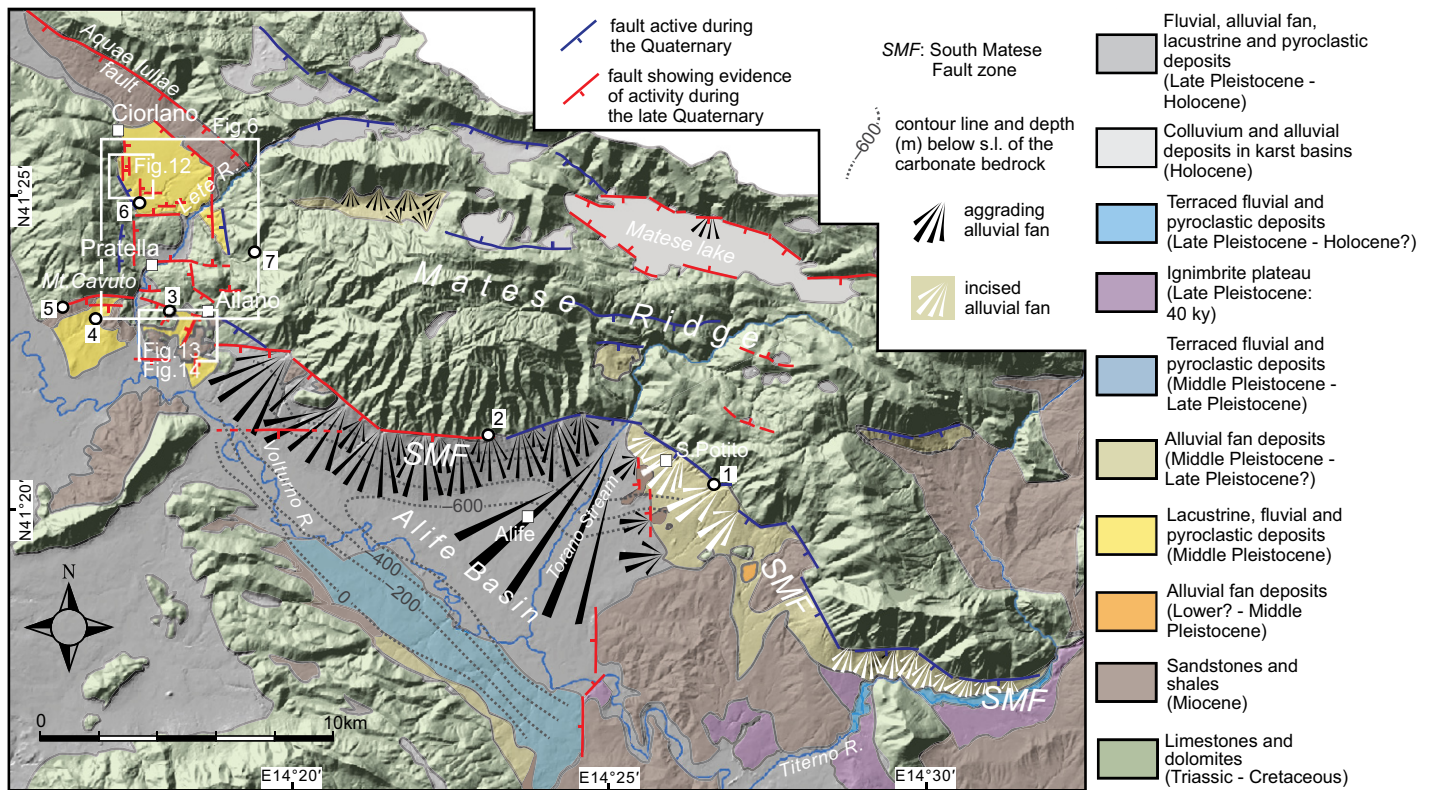
Figure 3. Simplified geological map of the study area overlying a 10 m digital elevation model derived from 1:5000 Regione Campania topographic maps, showing the South Matese Fault zone and faults with evidence of activity during the late Quaternary (location in Fig. 1). Contour lines and depth of the carbonate bedrock are from Corniello and Russo (1990). Location of sites discussed in the text and shown in the photos of Figure 4 are also included. The white boxes indicate locations of the maps shown in Figures 6, 12, 13, and 14.

the Titerno River (Fig. 3). Toward the west (i.e., in the San Potito area; Fig. 3) at least three generations of alluvial fans can be distinguished. The oldest one, which is exposed in a few outcrops from road cuts and quarries, consists of eroded conglomerates that have been dissected by faults and locally back-tilted (NE-dipping; Fig. 3). These first-generation alluvial fans are buried below large, incised second-generation alluvial fans that are composed of gravels and sands interlayered with volcaniclastic sediments and constitute the bulk of the piedmont alluvium (Fig. 3). In a quarry located at the toe of the Matese Ridge escarpment (site labeled 1 in Fig. 3), the contact between the deposits of one of these alluvial fans and the Mesozoic carbonates along a S-dipping fault is exposed (Fig. 4A). The western termination of the alluvial fans of the second generation is marked by a series of smooth and straight (~N-S–oriented) slope breaks that measure a few meters high. Below the slope breaks are active alluvial fan lobes of the third generation, which grade to the west to the Torano Stream alluvial fan (Fig. 3).

North of the Alife Basin, the piedmont is formed by an array of large alluvial fans that grade toward the Volturno River plain. The apexes of these alluvial fans are poorly indented into the mountain front and are slightly incised. An array of lobes is identified on the alluvial fan surfaces, pointing to recent aggradation of piedmont alluvium. In some quarries located at the boundary between the Mesozoic carbonate rocks and the alluvial fans, a network of mutually orthogonal, normal component E-W– and N-S–trending faults is exposed that dissect the carbonates. In one of these quarries (site 2 in Fig. 3), the contact between the top layers of the alluvial fan and the Mesozoic carbonates is exposed along a S-dipping fault plane.

To the north of the E-W–trending lineament that bounds the bajada (Ailano area; Fig. 3), the piedmont consists of a dissected, hilly landscape formed by Mesozoic limestones and Miocene sandstones that are overlain by Quaternary alluvial deposits composed of silts and clays as well as fluvial gravel and tephra layers, and tufa beds that are collectively classified as lacustrine facies. Alluvial deposits outcropping in the Ailano area are uplifted to ~150 m above the Volturno and Lete rivers alluvial plain (i.e., ~280 m a.s.l.) and are offset and locally tilted by E-W–, N-S–, and NE-SW–trending extensional faults (e.g., sites 3 and 4 in Fig. 3; Figs. 4B and 4C). The

surface expression of these structures is rather subdued, as topographic features in the Ailano area are also controlled by irregular, unconformable stratigraphic contacts among rocks with an inhomogeneous resistance to weathering (e.g., carbonates, sandstones, and clays/sands), and therefore essentially consists of faceted spurs that measure a few hundred meters in length and elongated ridges oriented primarily N-S and E-W. To the west of the Lete River valley, the Ailano lacustrine deposits are placed in contact with both the Mesozoic carbonates and Miocene sandstones by the south-dipping Mt. Cavuto fault (Fig. 3). Recent (Late Quaternary) activation of the Mt. Cavuto fault is inferred by the offset of talus breccia deposits that unconformably overlie the Ailano lacustrine succession (site 5 in Fig. 3; Fig. 4D).

Stream Profile Analysis

The degree of stream convexity varies progressively with location along Matese Ridge following an ~E-W trend (Fig. 5). Streams at the western (Streams 1, 2, and 4) and eastern (Streams 28, 32–34) ends of the ridge are primarily concave. Streams at the core of Matese Ridge (Streams 5–20) are primarily rectilinear
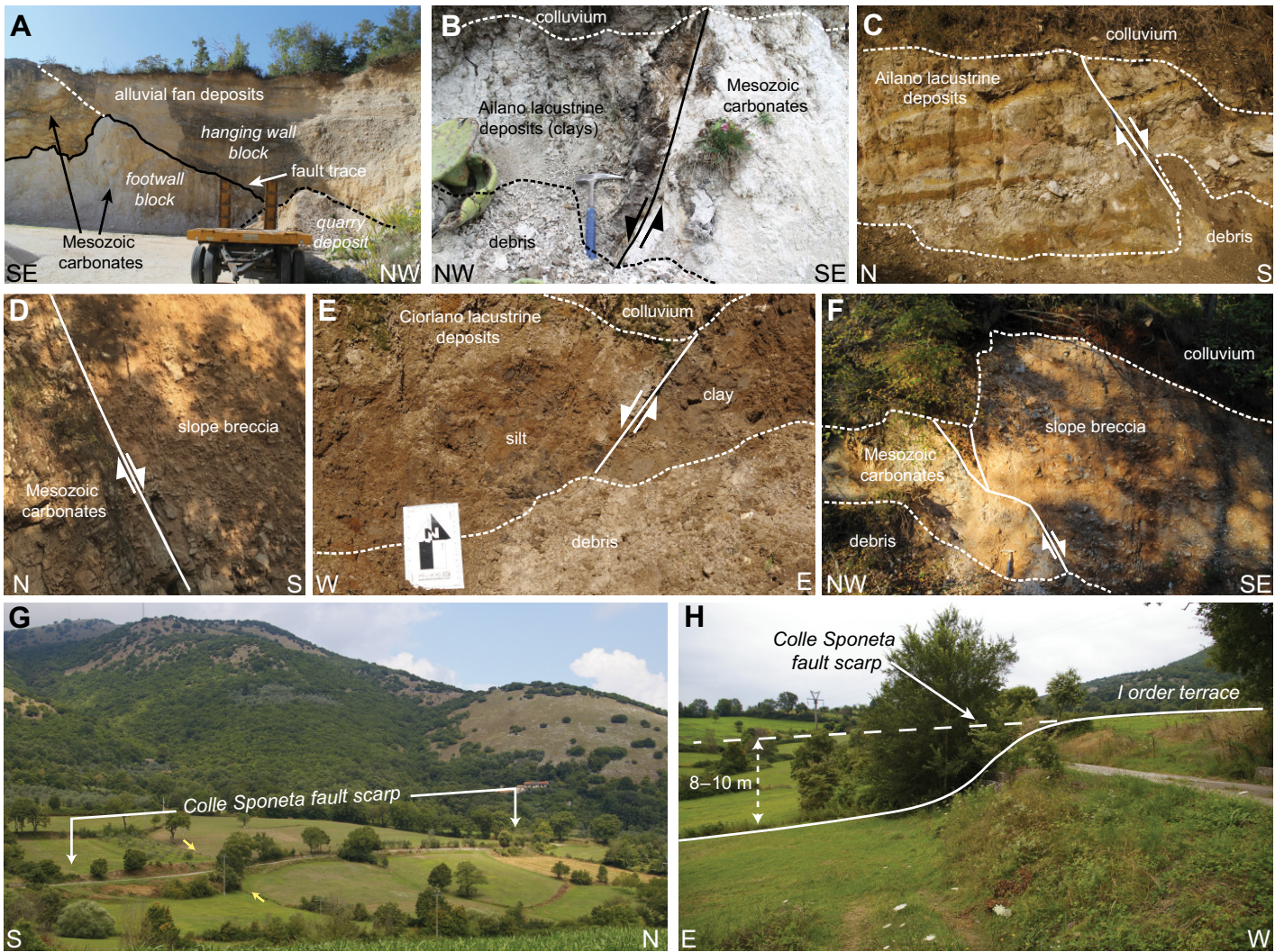
Figure 4. Quaternary deposits and terraces outcropping in the investigated area, offset by extensional faults (locations of outcrops shown in Fig. 3). (A) North-facing wall of the quarry of site 1 (located in Fig. 3) exposing the tectonic contact along a south-dipping fault plane between the Mesozoic carbonate rocks (in the footwall block) and alluvial fan gravels (in the hanging wall block). In the hanging wall block, the stratigraphic contact between the alluvial fan deposits and the carbonates is also shown. (B) Mesozoic carbonates and clays and silts of the Ailano lacustrine succession (Middle Pleistocene), placed in contact along an extensional fault plane dipping to the northwest (Site 3 in Fig. 3). (C) Silt, sand, and gravel layers of the Ailano lacustrine succession, offset by a south-dipping normal fault and tilted toward the north (Site 4 in Fig. 3). (D) South-dipping fault placing Mesozoic carbonates of the Mt. Cavuto ridge against loose deposits—probably Upper Pleistocene in age—forming the talus of the Mt. Cavuto southern fault scarp (Site 5 in Fig. 3). (E) Lacustrine clays and silts in the Ciorlano area, offset by a west-dipping fault (Site 6 in Fig. 3). (F) Tectonic contact along an east-dipping fault plane between slope breccia and Mesozoic carbonates (Site 7 in Fig. 3). (G) Frontal view of the N-S–trending, east-facing Colle Sponeta fault scarp (view from the east, location in Fig. 6). The fault scarp profile varies along strike from its natural convex shape to straight, which is probably due to the reworking of the area for agricultural purposes; yellow arrows indicate fault scarp profile shown in H. (H) View from the north of the east-facing Colle Sponeta fault scarp and offset first-order terrace, formed of Middle Pleistocene lacustrine deposits, shown in diagram C. White line follows topographic surface, dashed white line is used for rough quantification of surface displacement.

to convex with the most convex streams found in the central part of the dome-like structure of Matese Ridge. Streams that have incised around the domal feature to reach the local drainage divides of the internally drained basins (Streams 1, 2, and 4) are primarily concave in the west but have random convex upper reaches in the east (Streams 21–24). Streams north of this domal feature (Streams 5–6 and 18–20) are rectilinear to convex upstream and rectilinear to concave downstream, while streams along the southern flank (Streams 7–17) show a progressive increase in convexity toward the center of the dome. The sinking of the Torano Stream (Stream 24) east of the domal structure and the correlation between convex upper reaches and small basin-like features along the southeast range front suggest that karst processes may be dominant in the eastern part of Matese Ridge.

The group of internally-drained basins north of Matese Ridge can be subdivided into eastern and western parts along a primarily ~N-S drainage divide that roughly aligns with the center of the domal structure to the south (Fig. 5).
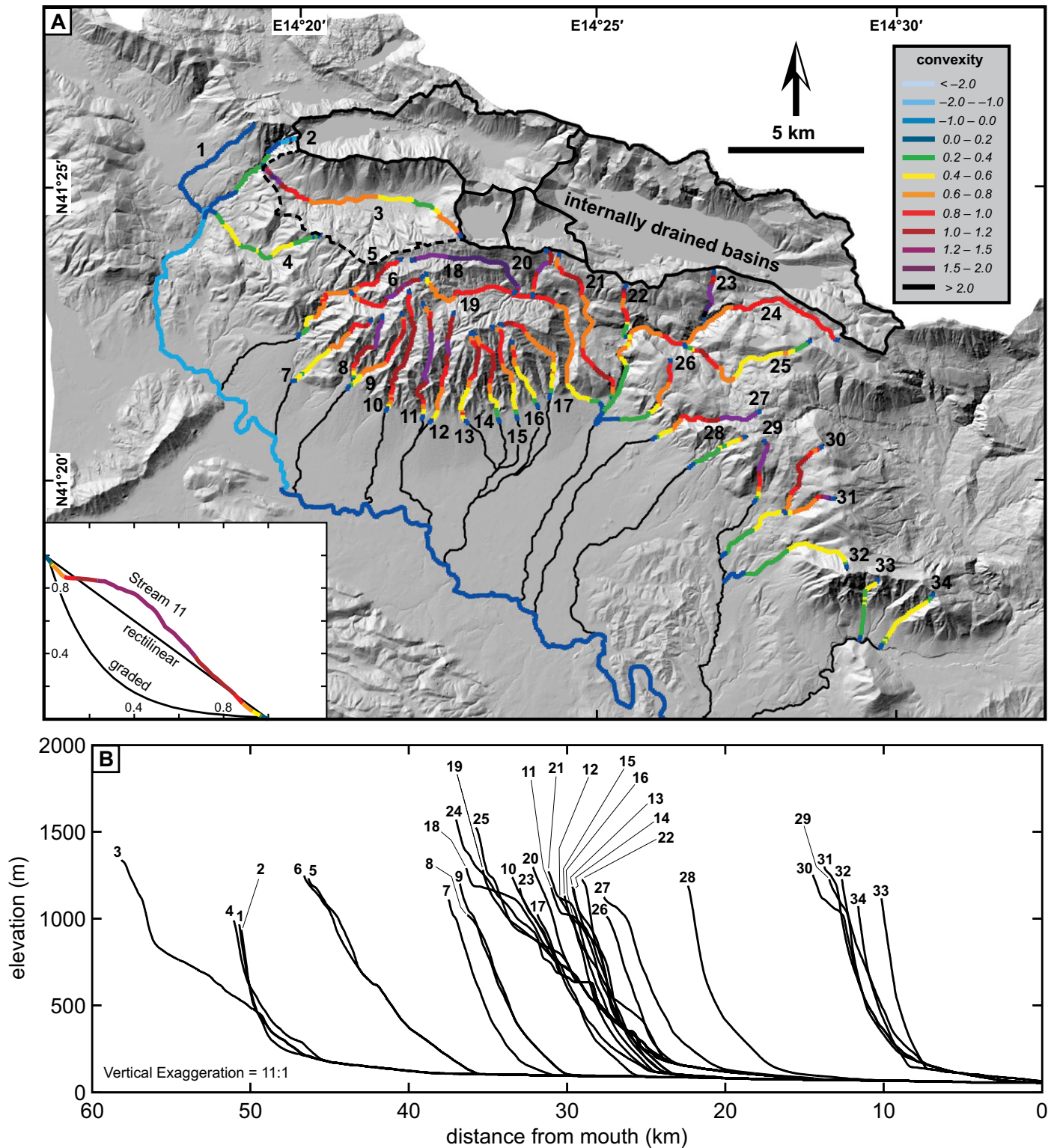
Figure 5. (A) Map of stream convexity data extracted from 10 m digital elevation model (DEM) derived from 1:5000 Regione Campania topographic maps and calculated using ArcGIS software. Black stream lines represent downstream reaches not analyzed by stream convexity method but included in stream profiles shown in diagram 5B. Internally drained basins outlined with solid black lines, catchment inferred to be breached internally drained basin shown with dashed black line (Stream 3). Inset diagram illustrates stream convexity method for Stream 11, with graded curve and rectilinear line serving as references for raw stream profile extracted from DEM. (B) Stream profile data extracted from 10 m DEM in ArcGIS and processed using stream profile tool (Whipple et al., 2007; http://geomorphtools .geology.isu.edu/Tools/StPro/StPro.htm).

Streams that have extended around the domal structure to reach the eastern and western ends of the internally drained basin area appear to be close to capturing these catchments despite a wide range in stream convexity, with Stream 3 most likely representing the past capture of one part of the internally drained basin area based on similar morphology to nearby basins and the notable steep reach at the outlet.

The Lete River Valley and the Ciorlano Area

The lower course of the Lete River flows across a flat alluvial plain. Within the alluvial plain, the Lete River initially follows a path of low sinuosity along the valley axis, while north of Pratella the river follows the left valley flank at marked bends.

North of Pratella, the Lete River alluvial plain is inset into terraced alluvial units. The highest terrace (first-order terrace in Fig. 6A) stands at 270–280 m a.s.l. in the Ciorlano area and is bounded to the west by a straight scarp formed in the carbonates. This terrace is composed of a succession of silts and clays interbedded with pyroclastic layers, which is dissected by N-S–trending faults (e.g., Site 6; Fig. 4E). The surface expression of these structures has created a network of subparallel, N-flowing streams that incise terraces and smooth scarps following a N-S trend (Fig. 6A). The most striking fault scarp (hereinafter referred to as the Colle Sponeta fault scarp; Fig. 6A) is an E-facing scarp measuring ~1 km long and up to 8 m high (diagrams F and G of Fig. 4). We correlate the first-order terrace in the Ciorlano area to the fill terrace standing at a comparable elevation

(~310–300 m a.s.l.) on the left flank of the Lete River valley (Fig. 6A). This terrace consists of coarse-grained fluvial pebbles that have been downfaulted to the east by an ~N-S–trending fault (Fig. 6A). To the east, a N-S–oriented fault places the carbonates in contact with slope breccia deposits (site 7 in Fig. 3). A lower, quasi-flat and incised depositional surface (second-order terrace, standing at a height of ~240 m a.s.l.) is inset into the first-order terrace. The second-order terrace, which is composed of silts interlayered with gravels and pyroclastic beds, extends laterally northward into incised alluvial fans (Fig. 6A). The sedimentary features of both the first- and second-order terraces reflect a lacustrine environment. Based on the spatial distributions of the first- and second-order terraces, the southern perimeter of the Ciorlano Basin paleo-lake may be placed along the northern
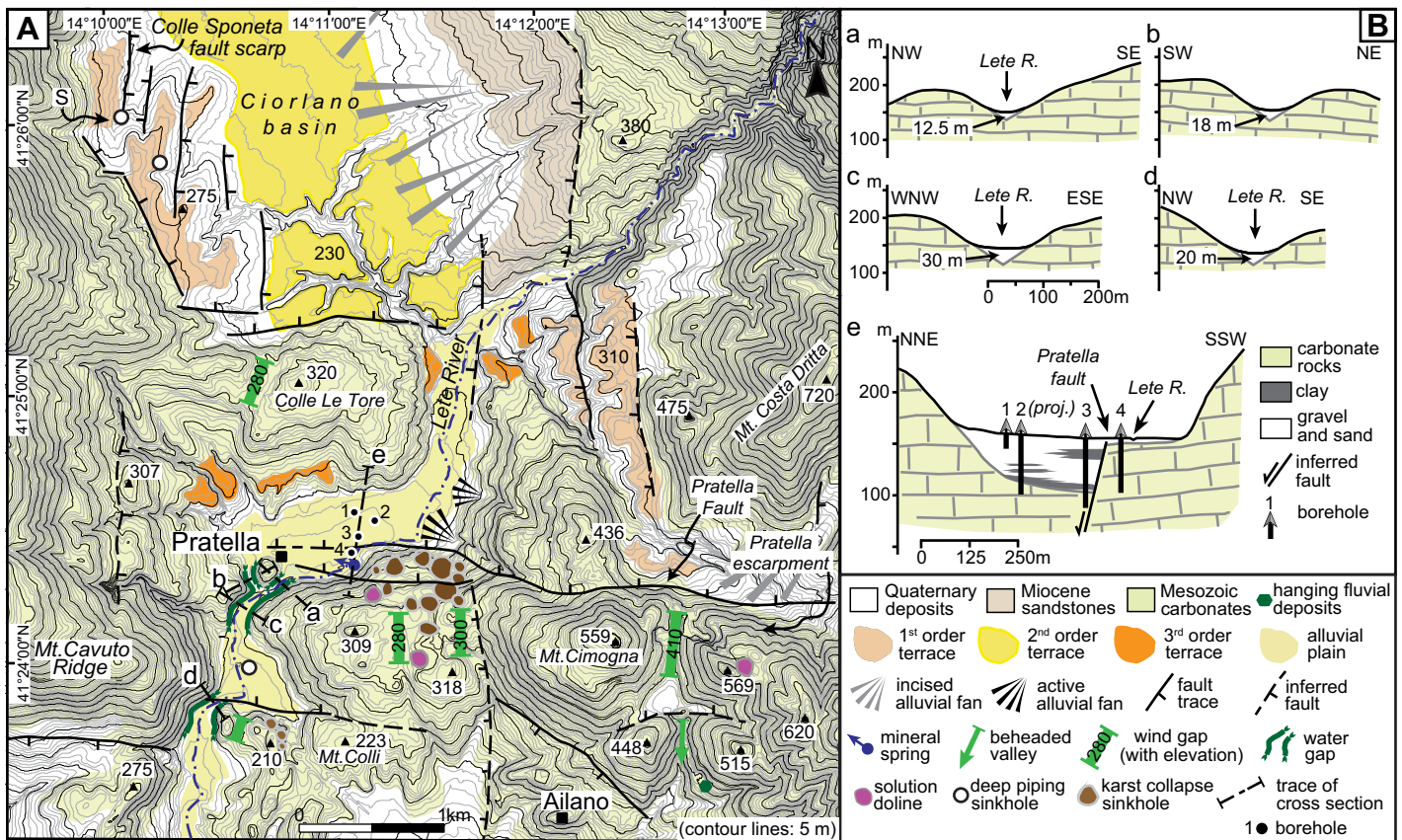
Figure 6. (A) Morphostructural map of the Pratella area (location in Fig. 3), plotted on the Regione Campania 1:5000 scale topographic map. The map shows (*i*) the fluvial/lacustrine terraces, (*ii*) the perimeter of the undissected Lete River alluvial plain and correlative alluvial fans, (*iii*) the relic (wind gaps) and present-day (water gaps) fluvial erosional landforms that are indicative of late Quaternary block-faulting, (*iv*) the solution dolines and collapse sinkholes formed in the carbonates and in the lacustrine deposits, (*v*) the sinkholes formed in alluvial deposits, and (*vi*) the traces of fault strands showing evidence of extensional activity during the late Quaternary. Traces of cross-sections in diagram (B) are also shown. (B) Geological cross sections of water gaps in the Lete River valley (locations in diagram A). Buried valley shapes and depths of valley bottoms (in meters) shown in cross sections a to d are inferred from dip angles of the valley flanks. Cross section e shows the sharp thickening of the valley fill to the north of the Pratella Fault trace, and cross sections a to d show that inferred valley depths are shallower than the thickest valley fill drilled to the north of the Pratella Fault.

escarpment of the incised carbonate ridges in the Colle Le Tore–Mt. Cimogna area (Fig. 6A), which appears to be the basin boundary. Hilltops of the Colle Le Tore–Mt. Cimogna blocks are characterized by karst topography (solution dolines filled by *terra rossa* deposits), while the northern escarpment of the Mt. Cimogna–Pratella block (hereinafter referred to as the Pratella escarpment; Fig. 6) and hilltop, as well as the Mt. Colli block more to the south, feature a dense distribution of karst collapse sinkholes (Fig. 6A). The Colle Le Tore–Mt. Cimogna block hilltops are also incised by wind gaps at elevations ranging from ~400–280 m (Fig. 6A). The original flow directions of the wind gaps are uncertain, however a patch of well-rounded pebbles located at ~360 m on the eastern flank of the beheaded valley trunk to the SE of Mt. Cimogna peak (location in Fig. 6A) provides evidence for south-flowing drainage of this area in the past. Among the wind gaps in the region, one SE of Mt. Cimogna peak terminates with a triangle-shaped basin that separates it from its former source area (i.e., the beheaded valley in Fig. 6A).

A third-order terrace consisting of small strath terraces cut into the carbonates and fill terraces formed by fluvial conglomerates is identified along the flanks of the Lete River valley at a height of ~30 m above the valley floor (~210–210 m a.s.l.; Fig. 6A). This third-order terrace may be correlated with the wind gap standing at a comparable elevation of 200 m across the Mt. Colli block (Fig. 6A).

The floor of the Lete River valley is characterized by an alternation of relatively wide and flat, undissected alluvial plain segments and water gaps (Fig. 6A). The widest valley segment is the reach that parallels the straight E-W–oriented Pratella escarpment. Published (Corniello et al., 1999) and unpublished borehole logs from the Pratella area (Fig. DR1[1]) point to the presence of a depocenter filled with alluvial deposits that covers an irregular surface likely formed by erosion of carbonate rocks. The presence of *terra rossa* interposed between alluvial fill and carbonates in some of the logs suggests that there may be buried karst landforms. The logs also show that the thickness of valley fill sharply increases to >50 m upstream of the Pratella escarpment (cross section e of Fig. 6B) and exceeds by some tens of meters the depths of

[1]GSA Data Repository item 2018150, Supplementary information includes the locations and logs of boreholes from the Pratella area (Figure DR1) and the list of the exploration wells from the southern Apennines in which CO_2 and CH_4 have been recovered (Table DR1), is available at http://www.geosociety.org/datarepository/2018 or by request to editing@geosociety.org.

the buried valley bottom found downstream in the water gaps that dissect both the Pratella and Mt. Colli blocks (cross sections a, b, c, and d of Fig. 6B). The occurrence of up to 10-m-thick beds and lenses of fine-grained and marshy deposits suggests intermittent ponding to the north of the Pratella escarpment.

SOIL GAS DATA

The two areas investigated by the soil gas survey, i.e., the Ciorlano site (~0.7 km²) and the Ailano site (~2 km²; Fig. 4), are characterized by a large number of gas vents recognized in the field by the scarce and/or total absence of vegetation, bubbling phenomena in water springs, and sinkholes associated with CO_2 emissions (Fig. 7).

Table 1 shows the main statistical parameters of the collected soil gas data. Soil gas CO_2 shows the highest concentrations within the SV and MV zones that exceed the upper threshold value typical of the soil at this latitude (ranging from 0.2 to 4%, Annunziatellis et al., 2008). Statistical results are also compared to the statistics of other volcanic and non-volcanic areas from the pan-Italian database produced over the past 30 years (Annunziatellis et al., 2008; Bigi et al., 2014; Ciotoli et al., 2016). An inspection of Table 1 highlights the very high mean (26.23%) and geometric mean (GM, 13.21%) values of CO_2 concentrations in soil gas of the Ailano site versus those calculated at the Ciorlano site (6.81% and 2.75% respectively). The Ailano site is also characterized by a very high concentration and flux of CO_2, caused by the widespread presence of gas vents (more than 200; see next Section). The histogram and the Normal Probability Plot (NPP) of Figure 8 highlight the presence of multiple statistical populations. In particular, many populations can be distinguished in the NPP: main vents (MV) from 75% up to the maximum value, secondary vents (SV) from 10 to 75%, diffusive zone (DZ) from 4.5 to 10%, and a background value from the minimum value to 4.5%.

The comparison of the concentrations of CO_2 with O_2 and N_2 in each of the samples analyzed in the laboratory provides a preliminary identification of the CO_2 source (Figs. 9A and 9B) (Beaubien et al., 2008; Romanak et al., 2012). In both figures, the alignment of samples along the leakage trend line toward 0% O_2/N_2 and 100% CO_2 clearly indicates that the addition of deep CO_2 to the system results in the dilution of O_2 and N_2. In Figure 9B, the samples to the right of the biological mixing line represent the addition of deep CO_2. The portable CO_2 analyzer made it possible to conduct a more complete coverage of the study sites and a quick assessment of deep

CO_2 input. Helium mean values are comparable at both sites (7.1 ppmv for Ciorlano and 6.6 ppmv for Ailano) and are higher than the helium (^4He) atmospheric content (5.220 ± 0.015 ppm, Holland and Emerson, 1990). Moreover, the maximum values measured at both sites are about ten times higher than the atmospheric value.
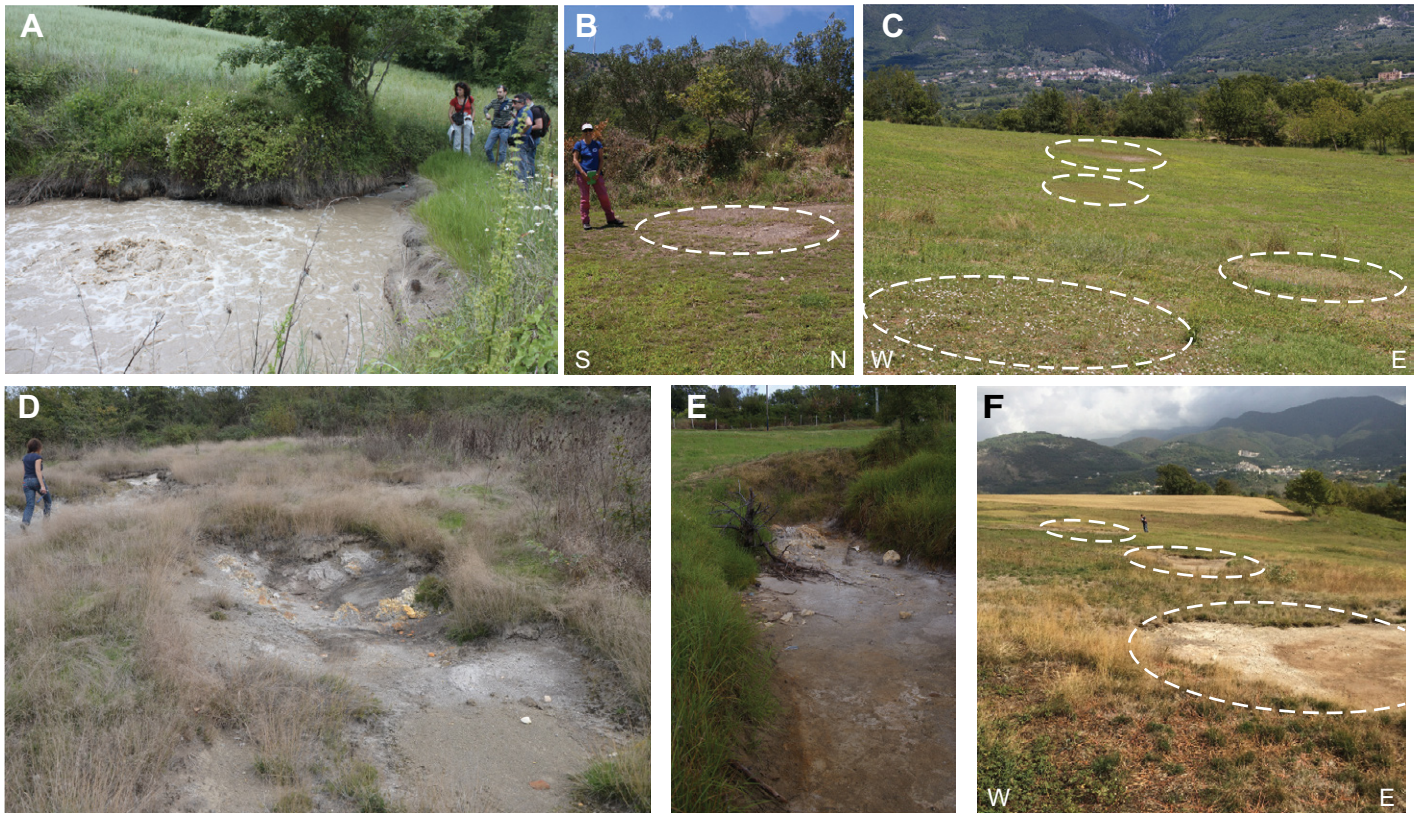
CO_2 Flux Measurements

A summary of the CO_2 flux statistics is reported in Table 1. The average CO_2 flux of the Ciorlano (103.60 g m^{-2} d^{-1}) and Ailano (1481 g m^{-2} d^{-1}) areas are about two and forty times higher, respectively, than typical normal soil systems (~40 g m^{-2} d^{-1}) reported by Beaubien et al. (2015). Similar to the CO_2 concentrations, the histogram and NPP plot of CO_2 flux also reveal multiple statistical populations both at the Ciorlano and Ailano sites (Figs. 10A and 10B). In particular, the NPP highlights the following: MV characterized by values >2000 g m² d^{-1} (diameters ranging from 10¹ to 10² m), SV with values from 500 to 2000 g m² d^{-1}, a diffusive flux far from the vents (DZ) ranging from 50 to 400 g m² d^{-1}, and a background biological flux from soil <50 g m² d^{-1}.

The higher sampling density around some of the larger leaking sites (10³–10⁴ g m² d^{-1}) allowed us to map in greater detail the extent of the high-flux zones. Furthermore, the CO_2 flux measured at the Ailano site is comparable with that measured in volcanic areas of northern Sicily, i.e., Vulcano Island and Mt. Etna (~10³ g m^{-2} d^{-1}; Carapezza and Granieri, 2004; Camarda et al., 2006; Gianmanco et al., 2007).

Gas isotope Results and Comparison with Other Non-Volcanic Emissions of Southern Italy

All gas samples collected from the gas vents of the Ciorlano and Ailano areas (both bubbling pools and soil gases) have a composition dominated by CO_2 (up to 98.40 vol%) with a minor concentration of CH_4 (up to 5000 ppmv). The stable carbon isotope composition of CO_2 ($\delta^{13}C_{CO_2}$: 2.95 and 1.30‰ VPDB for the Ciorlano and Ailano samples, respectively) is comparable with those previously published (Tedesco, 1997; Caracausi et al., 2013; Tassi et al., 2013), whereas the stable carbon isotope composition of methane ($\delta^{13}C_{CH_4}$) is –29.3 and –29.1‰ VPDB for the Ciorlano and Ailano samples, respectively. Furthermore, helium isotopes reported as R/Ra (R = $^3He/^4He$ of a sample and Ra is the ratio of these components in air: 1.39 × 10^{-6}) are also measured for use as a geochemical tracer for mantle-derived fluids (Lupton and Craig, 1975; Craig and Lupton, 1976).

Figure 7. Gas vents in the Ciorlano (photos A–C) and Ailano (photos D–F) areas. (A) Sinkhole to the south of the Colle Sponeta fault scarp (site S in Fig. 6), characterized by continuous and very abundant CO_2 flux that generates bubbles in this small lake (view from the south). (B) Gas vent, circled by dashed white line, at the toe of the Colle Sponeta fault scarp (view from the east). (C) Roughly N-S aligned gas vents (circled by dashed white lines) in the hanging wall block of the Colle Sponeta fault, located at a distance of a few tens of meters from the east-facing fault scarp (view from the south). (D) Large gas vents located to the southwest of Ailano. Note the intensely weathered clay and silt of the Middle Pleistocene lacustrine deposits (view from the southwest). (E) Gas vent to the southeast of Ailano (view from the west). (F) Succession of gas vents (circled by dashed white lines); in the foreground, the Ailano village is shown (view from the south).

The R/Ra is 0.89 for the Ciorlano samples and 0.99 for the Ailano samples.

The graph of Figure 11A shows the R/Ra values versus $\delta^{13}C_{CO_2}$ measured from the gas emissions of the Ciorlano and Ailano sites, and includes data from other non-volcanic gas vents of the southern Apennines for comparison (locations shown in Fig. 1). The volcanic R/Ra value of 6.22 from Mt. Vulture (sample 11, star) represents the highest value for the Apennines (Caracausi et al., 2013) and is similar to the value of the European subcontinental lithospheric mantle, ranging between 5.9 and 6.7 (Gautheron et al., 2005; Caracausi et al., 2013; Day et al., 2015; Brauer et al., 2016). The graph highlights that the Ciorlano and Ailano samples fall within the data range of other non-volcanic gas vents of the southern Apennines, which are characterized by R/Ra values ranging from 0.88 (Lete spring, Minissale et al., 2016) to 4.61 (Maschito, Caracausi, 2013) and $\delta^{13}C_{CO_2}$ values ranging from –1.90 (Terme Telese, Italiano et al., 2000) to 2.95‰ (Ciorlano). The highest

R/Ra values found from sample 13 (Maschito, Minissale et al., 2016) can be explained by magmatic intrusions at a depth of ~20 km linked to the Mt. Vulture magmatic system.

CO_2 and He isotopes indicate that all samples are influenced by a strong contribution of thermogenic CO_2 with variable amounts of mantle helium decreasing from the Mt. Vulture end-member and are derived from the magmatism related to the subduction of the Ionian/Adriatic plate below the Apennine chain (Tedesco, 1997; Martelli et al., 2004).

Figure 11B shows a plot of the stable carbon ($\delta^{13}C_{CH_4}$) and hydrogen ($\delta^2H_{CH_4}$) isotope composition of methane released from the main CO_2-rich manifestations in the southern Apennines, which range from –25.6 to –32.5‰ VPDB and –131 to –163‰ VSMOW, respectively. Overall, all methane from these CO_2-rich gases seems to have a dominant thermogenic origin (Td, dry thermogenic), but we cannot rule out that minor amounts of methane of abiotic origin (cogenetic with inorganic CO_2) may occur.

Spatial Distribution of CO_2 and CO_2 Flux in the Investigated Areas

The maps (2-D and 3-D; Fig. 12) of the CO_2 concentrations in the soil and of the CO_2 flux constructed for the Ciorlano site show a clear correlation between the N-S distribution of the highest leaking vents (MV and SV) and the Colle Sponeta fault scarp.

The maps (2-D, Fig. 13; 3-D, Fig. 14) of CO_2 concentrations in the soil and CO_2 flux of the Ailano area show a pattern similar to that of the Ciorlano site. Due to the very high number of MV and SV (~200) concentrated in a small area of ~2 km², the maps are constructed using equations of variogram models with a simple kriging algorithm (Figs. 13C and 14C). In particular, the experimental variogram calculated for the Ailano flux measurements (Fig. 14C) was modeled using nested models for a wide range of values (50–600 m). The data from the models indicates that fluxes are the expression of a phenomenon acting at two spatial scales,

TABLE 1. MAIN STATISTICAL PARAMETERS OF THE SOIL GAS AND FLUX DATA

	N	Mean	GM	Min	Max	LQ	UQ	10%	90%	Std. dev.
Ciorlano										
CO_2	229	6.81	2.75	0.14	76.00	1.60	4.40	0.80	8.70	14.47
fCO_2	181	103.60	32.90	2.87	2309	16.63	46.34	11.24	113.00	317.89
He	82	7.07	6.22	4.99	33.30	5.22	5.47	5.12	12.0	5.11
Ailano										
CO_2	346	26.23	13.21	0.07	98.40	1.80	56.00	1.11	89.30	34.40
fCO_2	346	1481	89.19	0.90	34159	14.80	526.87	8.74	3000	4464
He	77	6.58	5.36	1.32	52.12	4.97	5.44	3.02	8.44	6.59
CO_2 % other sites (Ciotoli et al., 2016)										
Ciampino	690	3.55	1.12	0.03	87.50	0.48	2.40	0.23	5.10	11.65
Fiumicino	1530	4.20	1.61	0.04	86.00	0.68	3.40	0.30	7.80	9.37
Volcanic areas	4860	3.33	0.88	0.03	100.00	0.41	1.92	0.18	4.81	10.32
fCO_2 (g m^{-2}d^{-1}) other sites (Bigi et al., 2014)										
Ciampino (Latium)	82	51.12	14.36	0.95	2206	7.87	22.85	6.28	35.87	17.51
Guidonia (Latium)	400	23.71	18.61	0.54	92.86	12.21	32.10	7.05	45.04	12.90
Latera (Latium)	1297	552.85	88.48	0.10	49564	24.10	293.00	8.00	890.00	2482

Note: CO_2 is expressed in %, v/v (volume per volume); He is expressed in ppmv (parts per million volume); CO_2 flux is expressed in g m^{-2}d^{-1}. N—number of samples; GM—geometric mean; Min—minimum value; Max—maximum value; LQ—lower quartile; UQ—upper quartile; 10%—10th percentile; 90%—90th percentile; Std. dev.—standard deviation.

with the advective leaks at MV and SV corresponding to variations at a short scale and the DZ acting at a larger scale. The distribution pattern of the peaks of both CO_2 concentrations and flux that are clearly visible on the 3-D maps defines two main anomalous zones oriented NE-SW and NW-SE, respectively. A N-S distribution of the MV and SV in the eastern part of the study area is also visible in the maps.

Distribution of Gas Emissions in the Matese Ridge Area and in Deep Wells

Figure 15 shows a map of the heat flow (mW m^{-2}; Della Vedova et al., 1991) and reports locations of sites listed in Table 2 as well as exploratory wells of the southern Apennines where CO_2 and CH_4 have been detected (data from the ViDEPI inventory; ViDEPI Project, 2010; Table DR1 [see footnote 1]). In some cases, boreholes report the local occurrence of CO_2 gas caps at the top of fractured Apulian carbonate reservoirs (Improta et al., 2014), while variable amounts of saline water are found along the sides of the structural traps and below the gas caps where present. Such a situation has been documented in the subsurface of the Mt. Forcuso ridge, where the strong gas emission of Mefite d'Ansanto is located (Inversi et al., 2013; Figs. 1 and 15). Only a few boreholes located to the east (Fig. 15) have detected CO_2 in the allochthonous units that overlie the Apulian Platform carbonates. An inspection of the map in Figure 15 highlights that most of the boreholes aligned along the axis of the mountain belt record the occurrence of CH_4 and CO_2 at depth and are overlain by areas of thermal anomalies, as indicated by the isotherms at a depth of 3000 m.
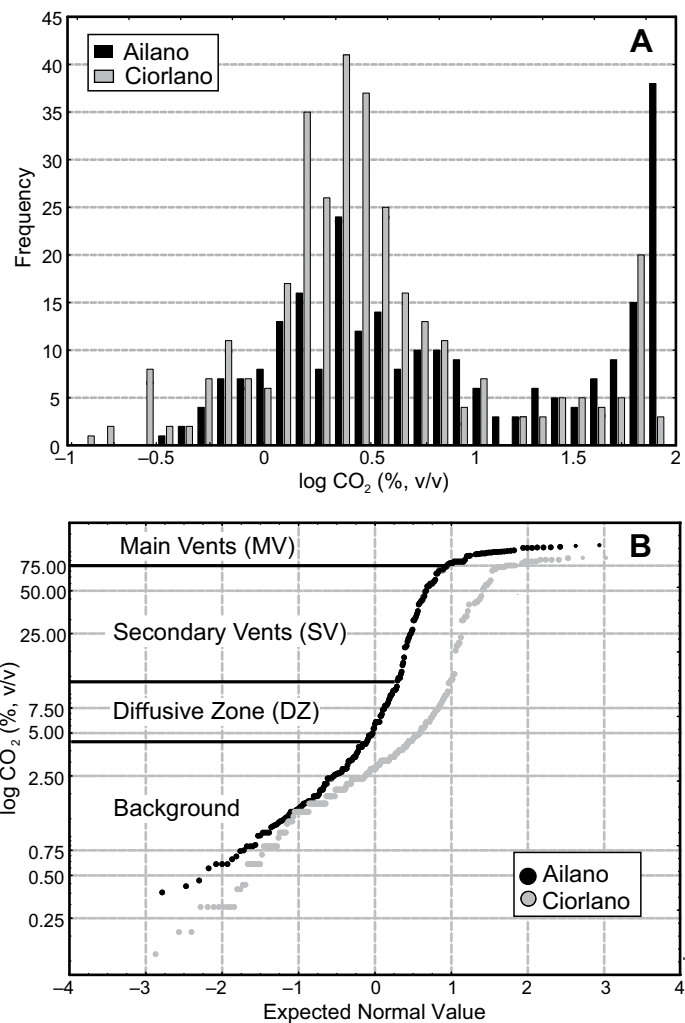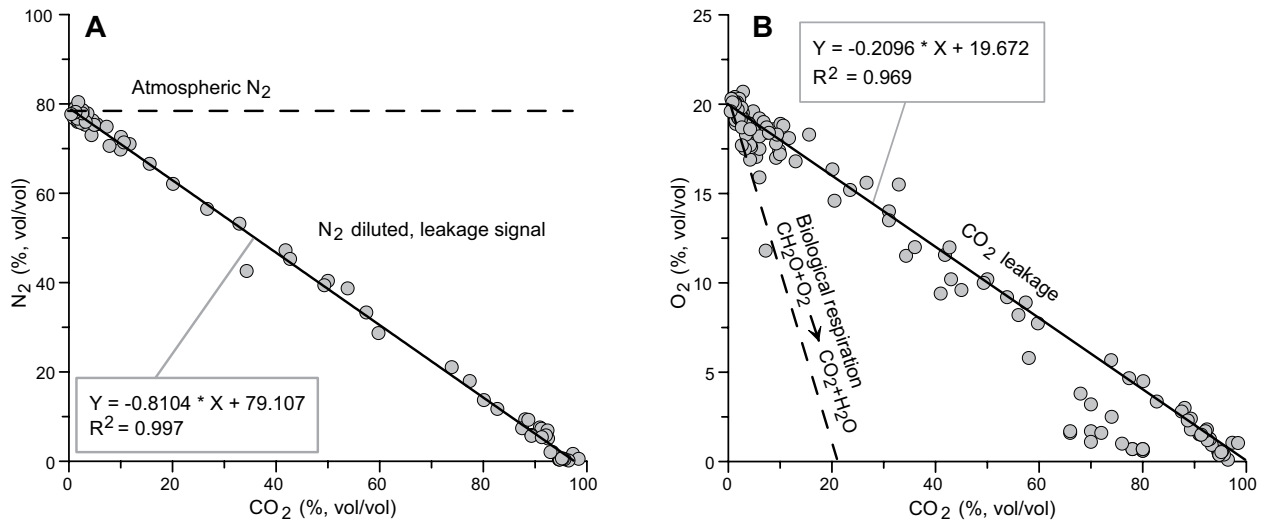

Figure 8. Histogram (A) and normal probability plot (NPP) (B) of CO_2 log-transformed data for Ailano (black bars) and Ciorlano (gray bars). The NPP shows the presence of multiple statistical populations: main vents (MV) > 75%, secondary vents (SV) from 15% to 75%, diffusive zone (DZ) from 4% to 15% and background values below 4% (Sinclair, 1991). v/v—volume per volume.

Figure 9. (A) CO₂ versus N₂ concentration for soil gas samples. Dashed line shows the atmospheric N₂ content. The decrease of N₂ below the atmospheric line indicates the N₂ dilution caused by deep gas input. (B) Plot of CO₂ vs O₂ concentration for soil gas samples. The dashed line indicates the biological respiration, whereas samples located along the continuous line highlight a dilution of O₂ by deep CO₂ input. vol/vol—volume per volume; R²—regression coefficient.

DISCUSSION

Late Quaternary Tectonic Framework

The tectonic geomorphology analysis points to the SMF as a major, long-lived structure that has produced a large offset. As is inferred from the topographic swath profile of Figure 1C and regional information, the SMF represents the northeastern limit of a series of downfaulted blocks that have been progressively lowered toward the SW, down to depths several kilometers below sea level (and underneath Calabrian to Holocene sediments more than 3000 m thick; Santangelo et al., 2017, and references therein) in the subsurface of the Campania Plain graben. Although part of the large vertical separation (~2000 m) between the southern peaks of Matese Ridge and the top of the carbonates in the subsurface of the Alife Basin could be partly inherited from the original Miocene to Pliocene fold and thrust belt, the presence of coupled surface and subsurface information, including the location of a continental basin (Alife Basin) in the hanging wall of the SMF, the displacement of Quaternary alluvial fan deposits in the piedmont (e.g., sites 1 and 2 of Fig. 3 and displacement of deposits of first-generation alluvial fans in the San Potito area) and overall geomorphological features of the mountain front, all point to Quaternary vertical motion along the bounding faults.

The symmetrical distribution of gross topographic features emanating from the central part of Matese Ridge appears to reflect the varying influence of geomorphological and tectonic processes on the landscape development of the region. The general surface morphology of the region varies from the center of Matese Ridge outward, with smoother, more subdued topography observed in the eastern and western parts of Matese Ridge, and rougher, more incised topography found at the center of the ridge, especially along the southern flank of the domal feature (Fig. 5). An opposite trend characterizes the piedmont area, where the less incised parts of the mountain front are faced by an array of incised, telescoped alluvial fans in the east (i.e., northern flank of the Titerno River valley and NE of the Alife Basin eastern boundary), and terraced lacustrine deposits in the west. However, the toe of the high mountain front north of the Alife Basin is characterized by aggrading alluvial fans that suggest the locus of alluvium deposition has been persistently located along the SMF in this area. This correlation typically reflects fault offsets accommodating alluvial fan deposition at uplifting mountain fronts (e.g., Bull, 2008), in agreement with evidence from the stream analysis.

The majority of streams in the region have a relatively short length and simple drainage pattern (i.e., generally low sinuosity) but there is a notable variation in stream spacing, with a sparse number of incised stream valleys characterizing areas in the east and west and the highest density of incised valleys along the southern flank of the domal structure. Streams with high convexities are relatively common throughout Matese Ridge, but a correlation appears to exist between stream location and degree of convexity. Streams with the highest convex-ity are primarily found framing the dome-like topographic feature along the southern part of Matese Ridge, which includes ~N-S–trending streams that flow down the southern flank of the dome to the middle of the Volturno River valley (Streams 7–17) and ~E-W–trending stream reaches on the northern boundary of the dome that ultimately flow ~southward to the Volturno River (Streams 5–6 and 18–19) (Fig. 5A). In contrast to streams from the central part of Matese Ridge, stream profiles exhibit a progressive decrease in convexity extending east and west of the dome structure (Figs. 5A and 5B). Stream profiles from the relatively steep mountain front to the southeast of Matese Ridge (Streams 28 and 32–34) are concave or have reaches with only a low to moderate degree of convexity (Figs. 5A and 5B).

The progressive increase in stream convexity toward the center of Matese Ridge both along the southern flank of the dome and at the drainage divide separating the east-west reaches of the streams to the north suggest that the force driving stream convexity may emanate from the center of the domal feature (Figs. 5A and 5B). If convex stream reaches represent surface uplift that has outpaced fluvial downcutting as has been inferred in other locations in the Apennines (e.g., Whittaker et al., 2007, 2008; Ascione et al., 2013), then the domal feature may represent a locus of either recent or fast surface uplift, consistent with evidence from alluvial fan morphology in the same area.

Complementing evidence for recent surface uplift in the central part of Matese Ridge is the subsidence and ponding of the Alife Basin,
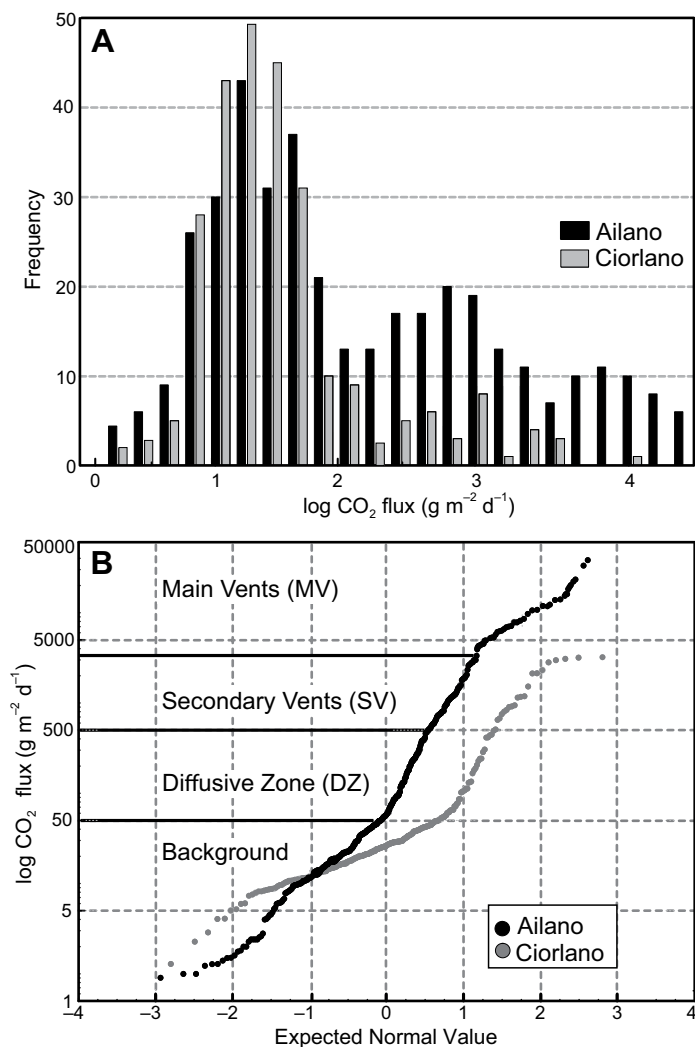
Figure 10. Histogram (A) and normal probability plot (NPP) (B) of the CO_2 flux log-transformed data for Ailano (black bars) and Ciorlano (gray bars). The NPP shows the presence of multiple statistical populations: main vents (MV) 10^3–10^4 g m^{-2} d^{-1}, secondary vents (SV) 10^2–10^3 g m^{-2} d^{-1}, diffusive zone (DZ) 10^1–10^2 g m^{-2} d^{-1}, and background values 10^1 g m^{-2} d^{-1} (Sinclair, 1991).

which is inferred from both the presence of Holocene lacustrine deposits in the Alife area and the recent basinward shift of alluvial fan deposition (third-generation alluvial fans) in the eastern boundary of the basin. Such information along with the displacement of the uppermost alluvial fan beds in the bajada (site 2 in Fig. 3) point to recent offset along the central segment of the SFM.

Both surface and subsurface information suggests that the eastern boundary of the Alife Basin, which is marked by the sharp rise of pre-Quaternary bedrock along ~N-S–oriented straight scarps (Fig. 3), follows a W-dipping extensional fault. In the west, the carbonate bedrock tends to rise gradually toward the Ailano area, where

it crops out beneath Miocene sandstones and the Ailano lacustrine deposits. The latter deposits may be chronologically bracketed within the Middle Pleistocene based on the presence of pyroclastic layers in the lacustrine succession and on the amount of incision (up to ~150 m) of their top surfaces. The Ailano lacustrine deposits have a composition (silt and clay interlayered with gravel, pyroclastic deposits, and tufa beds) that is comparable to deposits buried in the subsurface of the Alife Basin. Based on this similarity, the Ailano lacustrine deposits likely represent a raised portion of the Alife Basin fill, which have been uplifted by the ~E-W structure that marks the boundary between the deposits to the north and the bajada to the south.

The relative age difference between the lacustrine deposits outcropping in the Ailano and Ciorlano areas is not clear. However, the degree of preservation of the highest terraces in the Ciorlano basin area is better than that of terraces in the Ailano area, and the drainage direction inferred from hanging valley fluvial deposits to the south of the wind gap that is incised at around 400 m a.s.l. at the Mt. Cimogna ridge suggest the Ailano lacustrine deposits may predate deposits of the first-order terraces in the Ciorlano basin. The straight planform views of the escarpments to the north of and within the Colle Le Tore–Mt. Cimogna blocks, the relic drainage found on the hilltops of these blocks and the arrangement of terraced units in the Ciorlano Basin point to uplift of the Colle Le Tore–Mt. Cimogna block as a primary driver for controlling valley damming phenomena and depocenter distribution in the Ciorlano area during the Middle Pleistocene. Repeated activity of the ~E-W–trending faults that frame and dissect the Colle Le Tore–Mt. Cimogna block may have led to the establishment of internal drainage features in the Ciorlano area, which may also be reflective of activity of the ~N-S–trending faults found along the eastern and western boundaries (e.g., Colle Sponeta area). Early activation of the E-W–trending faults postdates incision of the wind gap on the Mt. Cimogna hilltop at 410 m a.s.l., while the wind gaps at 280–300 m suggest that open drainage was reestablished in response to the filling of the Ciorlano Basin with alluvial deposits that are found in the first-order terraces. The concurrent activation of orthogonal fault segments (having ~E-W and ~N-S trends) postdating the formation of first-order terraces may be represented by the deposition of the second-order terrace alluvium, possibly in the late part of the Middle Pleistocene. Renewed open drainage conditions along the Lete River valley are inferred from incision of the second-order terraces and formation (possibly still in the late part of the Middle Pleistocene) of both the third-order terraces and the wind gap in the Mt. Colli block. Activation of the Pratella fault array postdating the third-order terrace is inferred from the net increase of valley fill thickness (exceeding valley depths in the water gaps that incise the Pratella and Mt. Colli blocks) and intermittent ponding upstream of the Pratella fault. Recent valley damming by N-dipping fault strands is also inferred from the triangular-shaped valley segments to the north of both the Mt. Colli and the beheaded valley to the southeast of Mt. Cimogna peak.

Taking all of the geomorphological and stratigraphical data into consideration, the southern flank of Matese Ridge seems to represent the topographic expression of a tectonically active

Figure 11. Isotopic values from this work and from published data. (A) He isotopic ratios (R/Ra) versus $\delta^{13}C_{CO_2}$ of the southern Apennines areas from different authors (see Table 2) compared with other gas manifestations in the Latium Roman Comagmatic Province (L-RCP). RCP mantle data from Tedesco (1997) and Martelli et al. (2004); mid-ocean ridge basalt (MORB), marine limestone, and organic sediments are from Sano and Marty (1995). Mixing lines are among limestone, sediment and L-RCP end-members; the latter (R/Ra ~1) inferred from Martelli et al. (2004). All data are compared with the European sub lithospheric mantle (ESLM) (Gautheron et al., 2005). (B) $\delta^{13}C$-CH_4 versus δ^2H-CH_4 diagram for the gas discharged in the southern Apennines from different authors (Table 2) and in the closest manifestations surrounding Rome (Latium-RCP). Genetic CH_4 fields are from Etiope et al. (2011) and Etiope and Sherwood Lollar (2013). M—microbial; M.C.R.—microbial CO_2 reduction; M.A.F.—microbial acetate fermentation; T—thermogenic; To—thermogenic with oil; Tc—thermogenic with condensate; TD—dry thermogenic; TLM—thermogenic low maturity; A—abiotic; PC—Precambrian crystalline shields; GV—geothermal-volcanic systems; S—serpentinized ultramafic rocks; VPDB—Vienna Pee Dee belemnite; VSMOW—Vienna standard mean ocean water.
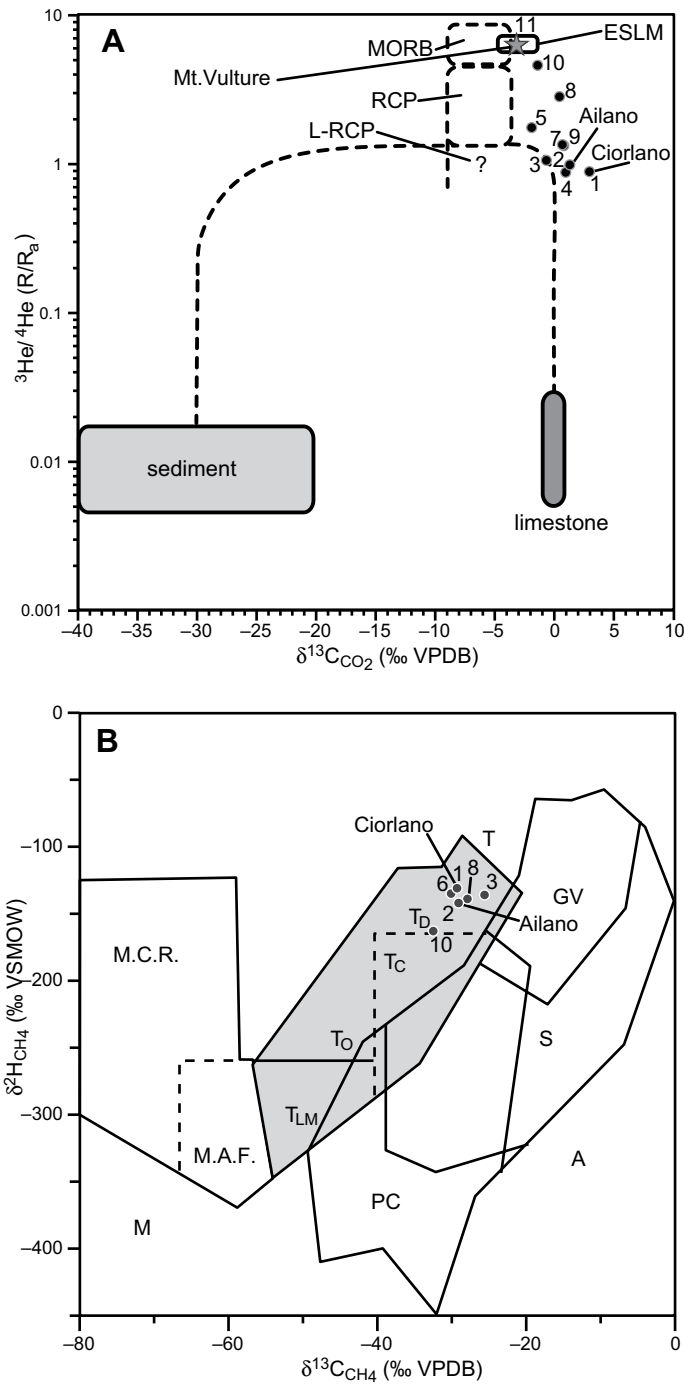

mountain front. This inference is noteworthy considering that the profile of the southern flank of Matese Ridge is steeper than that of the northern flank, which is bounded by the northern Matese fault system with evidence for Holocene activity (Galli et al., 2017). Late Quaternary slip along the SMF does not equate to uplift along the entire mountain front, which is also supported by the pattern of deposition in the piedmont. The offset of young alluvial fan beds and undissected alluvial fans suggest that the most recent activity of the SMF occurred along the fault strand bounding the southern flank of the dome structure, while displacement of Middle Pleistocene alluvial fan deposits and incised alluvial fans in the southeast likely represent a former locus of tectonic activity or slower fault motion. The stream profile convexity data provide additional evidence for the topographic response to tectonic activity along the SMF further back in time, and consistent with the geomorphological and stratigraphical data, the distribution of high stream convexities suggests that tectonic activity has occurred more

recently near the center of the southern flank of the domal structure. Furthermore, evidence for ponding and lacustrine deposition in the Alife basin during the Holocene suggests that activity of the central segment of the SMF has continued over the last few thousand years.

In the Ailano–Ciorlano area, a particularly dense network of small extensional fault strands (ranging from <1 kilometers to a few kilometers in length; Figs. 3 and 6) active during the late Quaternary has been identified. Although

the last activation of these fault segments is difficult to assess based on limited information about fault offsets found in undated sediments or primary erosional landform features (i.e., fault scarps formed in lacustrine deposits), a Holocene age may be inferred for at least the activity of the N-dipping structures. In the area surrounding Pratella, these N-dipping structures have controlled the damming of the current Lete River valley and the bends in the Lete River path, which suggest the response of the drainage net-
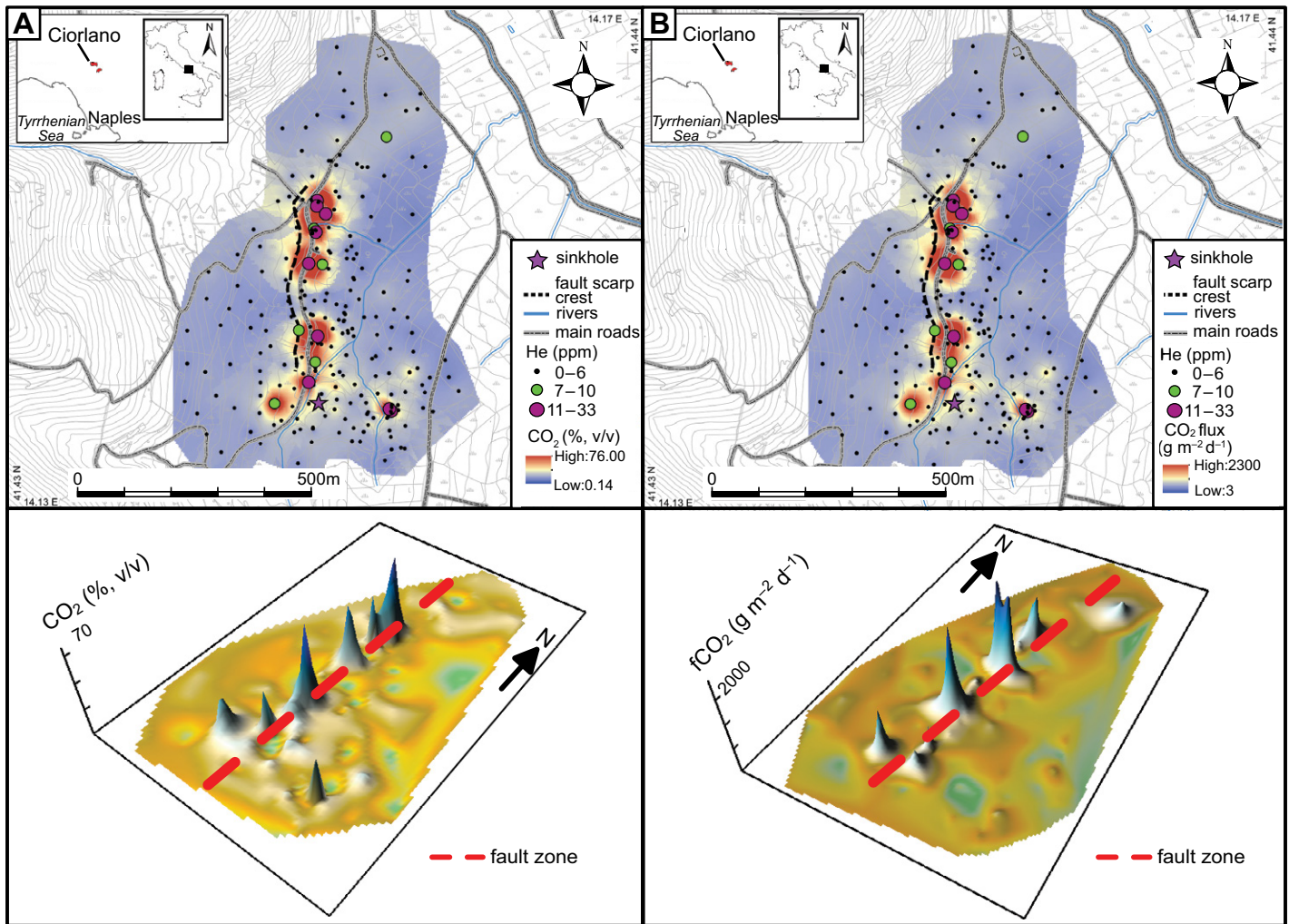
Figure 12. 2-D and 3-D soil gas CO$_2$ (A) and CO$_2$ flux (B) spatial distribution at the Ciorlano site. The distribution of both CO$_2$ concentration and flux as well as the He concentration in soil gas (violet and green circles) highlight the anomalies clear alignment along the N-S–trending Colle Sponeta fault scarp, as shown in the 3-D plot and in diagrams G and H of Figure 7. v/v—volume per volume.

work is highly reactive to slight changes in gradient along the valley floor due to downfaulting along the Pratella fault (Figs. 3 and 6). Orientations (NE-SW, N-S, and E-W) of fault strands in the Ailano–Ciorlano area parallel those of older structures that dissect the Mesozoic carbonates throughout Matese Ridge. Evidence for late Quaternary reactivation of fault strands inherited from earlier stages of the structural evolution of the thrust belt within the present day stress field (which is characterized by NE-SW–oriented horizontal extension) but originally acting with different kinematics is widespread in Matese Ridge (e.g., Butler et al., 2004) and is common throughout the southern Apennines (e.g., Cello and Mazzoli, 1998; Caiazzo et al., 2006; Macchiavelli et al., 2012; Vitale et al., 2012; Ascione et al., 2013). The dense fault network in the Ailano–Ciorlano area, which overlaps with the transient area between two major fault zones

(the SMF to the SE and the Aquae Iuliae fault to the NW), could be interpreted as a transfer zone (sensu Morley and Wonganan, 2006) or a broken relay ramp located in a step area.

Spatial distribution of gas emissions and source of the emitted gases

Strong gas manifestations occur as MV and SV (at the Ailano site we have measured only 80 out of ~200 in an area of ~2 km^2), and the diffuse emissions (DZ) should be added to this quantity. Such a large amount of CO$_2$ degassing is comparable to that measured in active volcanic areas making this area quite unique for Italy in terms of gas vent density and total flux emission, with a preliminary discharge estimate of ~500 t d^{-1}. The emission of large quantities of CO$_2$ is also demonstrated by the presence of mineral springs (e.g., Acqua Lete, one of the most popular bot-

tled mineral water companies in Italy, produces ~440 million litres/yr from these springs). As is shown in Table 1, mean values of CO$_2$ at both sites (including both advective and diffuse components) are very high if compared with mean values measured at volcanic areas of central and southern Italy (6.81% and 26.23% versus 3.33%, respectively). In fact, the composition of the soil gas concentrations measured at the MV, corrected for air content, indicates that the gas source depth primarily consists of up to 99 vol% of CO$_2$, up to 0.55 vol% of CH$_4$, and up to 52 ppmv of He.

CO$_2$ flux, measured along with the gas vents and surrounding zones, also shows a magnitude comparable and/or higher than that measured at Volcano Island in northern Sicily (10^3–10^4 g m^{-2} d^{-1}) (Carapezza and Granieri, 2004; Camarda et al., 2006). Maps in Figures 12 and 13 show localized main gas vent alignments that, at the
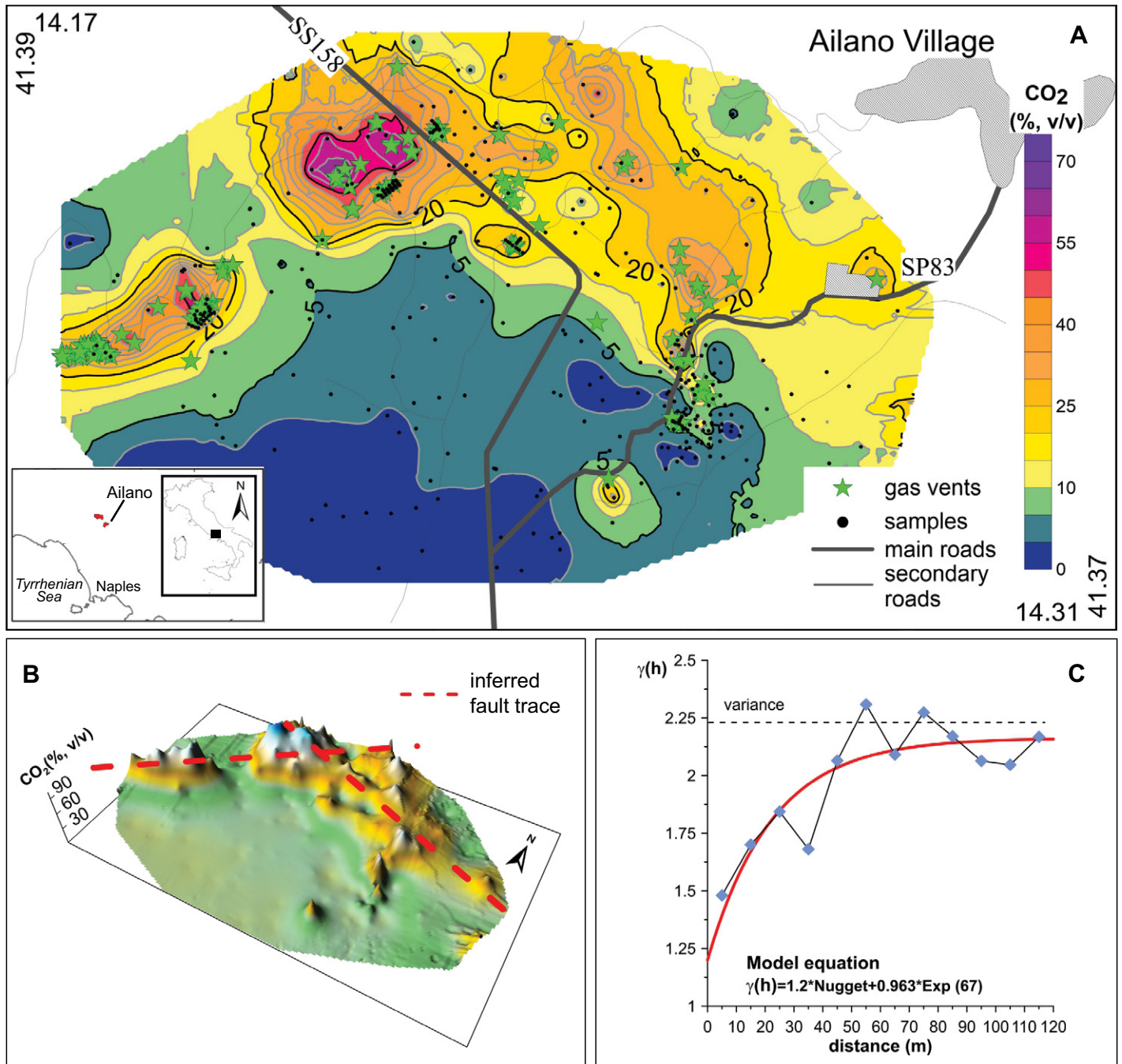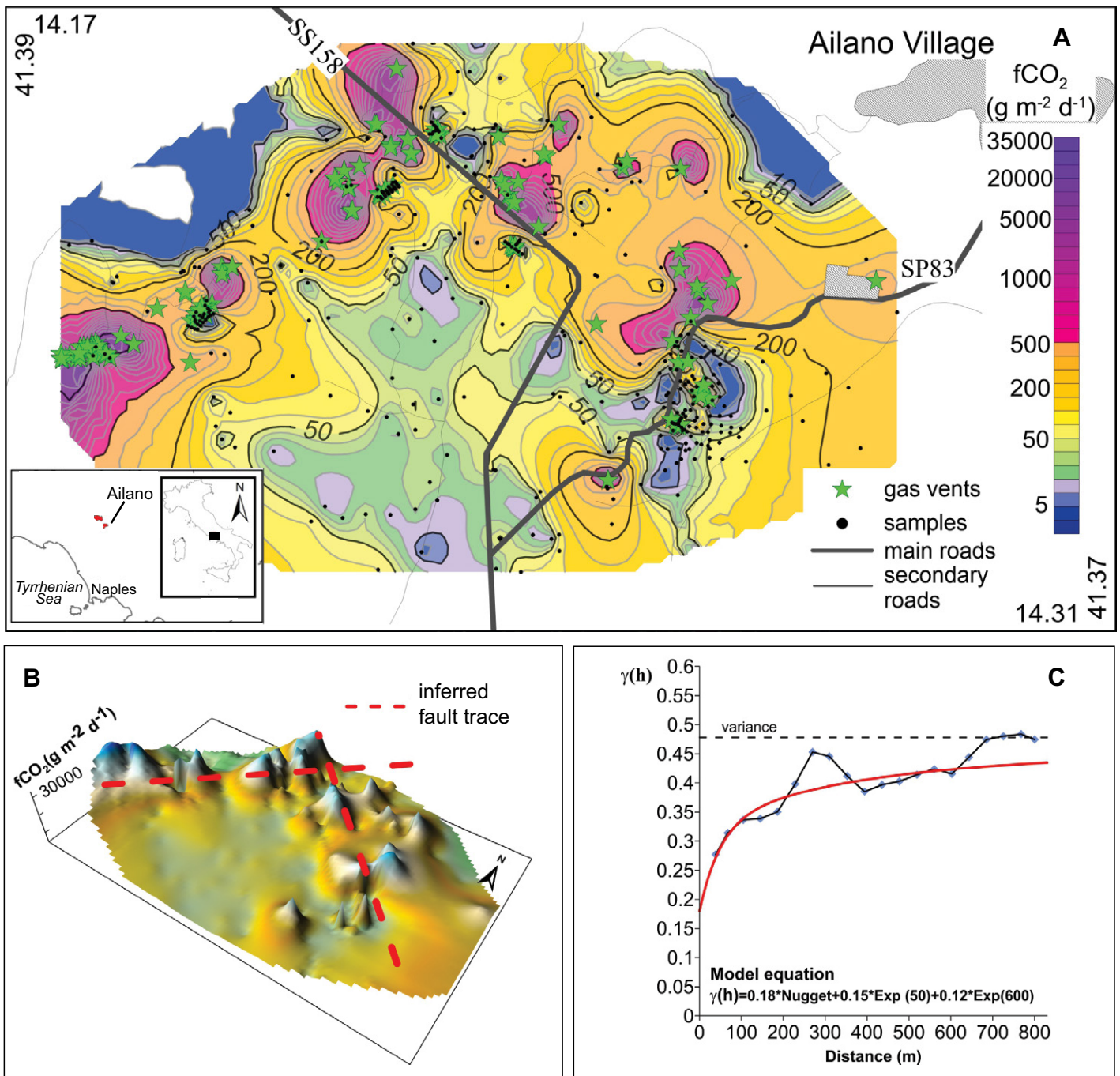
Figure 13. 2-D and 3-D maps of the estimated CO_2 concentrations in soil gas (A and B) obtained by kriging interpolation and the experimental variogram with the model equation used in the kriging algorithm (C) in the Ailano area. The map also shows the location of measured main gas vents (green stars). The 3-D map highlights the ENE-WSW– and WNW-ESE–oriented distribution of the CO_2 peaks. The variogram shows a good spatial autocorrelation of the CO_2 concentrations up to a range of ~70 m. v/v—volume per volume.

Ciorlano site, are surrounded by belts of very high diffuse gas emissions. The distributions of both gas vents and diffusive anomalies are localized in a region that is dissected by a dense number of fault strands that exhibit evidence for activity during the late Quaternary. Furthermore, the gas vent alignments are consistent with orientations of fault segments active during the late Quaternary in the study area. In particular, anomalous concentrations and flux values of CO_2 at the Ciorlano site, which also correspond to high He concentrations in soil gas, clearly follow the N-S–oriented Colle Sponeta fault scarp. These observations suggest that both gas vents and anomalous diffuse emissions are strongly controlled by the fault network, which is able to maintain a high structural permeability along strike. Furthermore, the presence of high concentrations of He (above the 90th percentile, ~8 ppmv) coupled with high concentrations of thermogenic CO_2 in correspondence with the MV, may indicate that fluids are rising from a source at depth along the faults, such as those located in the southern Matese Ridge area.

Figure 14. 2-D and 3-D maps of the estimated CO$_2$ flux values (A and B) obtained by kriging interpolation and the experimental variogram with the model equation used in the kriging algorithm (C) in the Ailano area. The map also reports the location of the measured main gas vents (green stars). Note the very high density of gas vents clustered in a relatively small area. As for the CO$_2$ concentration map, the 3-D map of the CO$_2$ flux also highlights the ENE-WSW and WNW-ESE distribution of the CO$_2$ peaks. A north-south distribution of the main vents (MV) and secondary vents (SV) in the eastern sector of the Ailano area, which is also visible on the maps, aligns with the inferred fault with a N-S trend that dissects the Mt. Cimogna block (Fig. 6). The experimental variogram was modeled by using nested models with different ranges (50 and 600 m, respectively), thus indicating that CO$_2$ flux distribution is the expression of a phenomenon acting at a dual spatial scale, with the advective leaks at MV and SV corresponding to the short scale variation of ~50 m and the diffusive zone acting at a larger scale of up to 600 m.
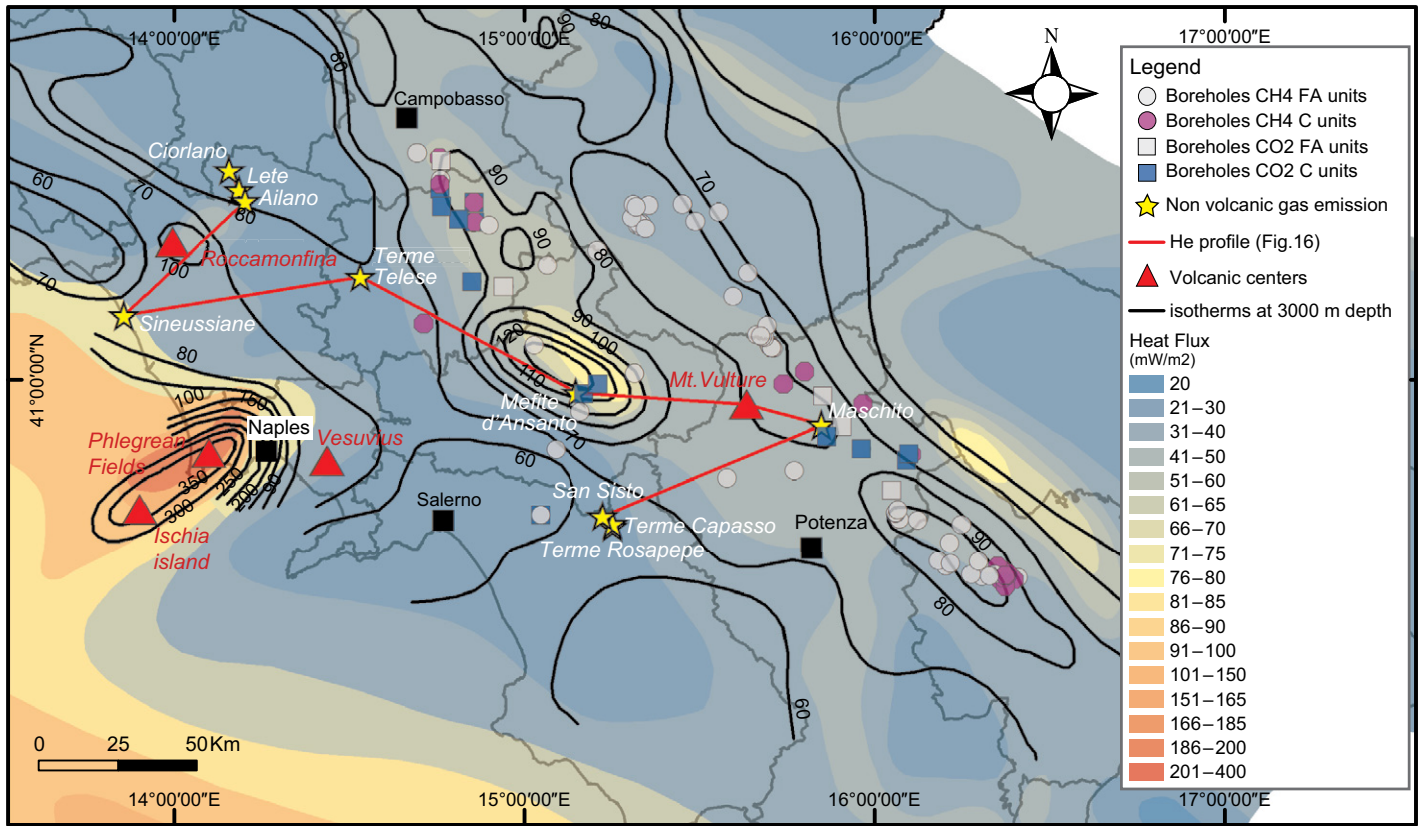
Figure 15. Heat flow map of the southern Apennines region (redrawn from Della Vedova et al., 1991), showing non-volcanic gas emissions sites with isotopic gas data from both this work and the literature, and locations of exploration wells characterized by the presence of CO₂ and CH₄ (data extracted from the ViDEPI database; ViDEPI Project, 2010). Mapped boreholes are grouped into four classes based on the presence of CH₄ in the Apulian Platform carbonate rocks (purple circles) and in the allochthonous cover (empty circles), and/or the presence of CO₂ in the Apulian Platform carbonate rocks (blue squares) or in the allochthonous cover (empty squares). Isotherms at a depth of 3000 m are also shown (data extracted from Geothopica Project; http://geothopica.igg.cnr.it/). The red line corresponds to the trace of the profile in Figure 16.

The same scenario can be assumed for the Ailano site, where the distribution of gas emissions appears to be more articulated due to a high number of MV, which are probably linked with a more complex and densely distributed fault network affecting the region that is much closer to the SMF. There, the NE-SW, NW-SE, and N-S alignments of the MV and SV suggest there are underlying gas-permeable faults with the same orientations.

The CO_2 flux distribution shows sharper anomalies with high values in the core of the MV and SV relative to surrounding areas, and a spatial distribution of anomalous values that decrease rapidly away from the core leak point (Figs. 12 and 14). This implies, as is commonly observed, that advective leakage occurs in a restricted area around the core of the gas vent, where the sediment properties have been locally compromised, while the areas surrounding the gas vent core are characterized by a diffusive flux strongly affected by soil properties such as

soil type, porosity, moisture, etc. (Annunziatellis et al., 2008). The degradation of sediment and rock properties associated with advective leakage of acidic fluids and associated enhanced weathering appears to be the causative mechanism for the formation of the high number of deep piping sinkholes (e.g., Caramanna et al., 2008) and karst collapse sinkholes (e.g., Santo et al., 2011) that affect the Quaternary alluvial units and Mesozoic carbonates, respectively. It is worth noting that karst collapse sinkholes are clustered along both the Pratella fault and Mt. Colli fault, suggesting localized gas emissions (not directly measurable in the thin soil cover overlying the carbonates) may also be associated with these structures.

Isotopic data from Ciorlano and Ailano gas samples have been integrated with those of other gas manifestations of the southern Apennines available in the literature for a better understanding of the gas source (Magro and Pennisi, 1991; Tedesco, 1997; Minissale, 2004; Googas,

2006; Rizzo et al., 2006; Italiano et al., 2010; Vaselli et al., 2011; Tassi et al., 2012; Caracausi et al., 2013) (Table 2). Carbon ($\delta^{13}C$) isotopic values of CO_2 for Ailano and Ciorlano samples (1.3‰ and 2.95‰, respectively) both fall in the range of limestone decarbonation that often reflect a crustal gas source with only subordinate mantle component. However, slightly negative $\delta^{13}C$ characterizes the gas emission of the Roccamonfina and Vulture magmatic systems, and for this reason helium R/Ra is also considered since it provides a better discrimination of the gas source (e.g., mantle vs crustal). The R/Ra has been compared with the magmatic value measured at Mt. Vulture (Caracausi et al., 2013), which is considered to be an approximation of the end-member of the lithospheric mantle-He signature beneath the Apennines thrust belt. Figure 16 shows the NW-SE mantle-derived He enrichment along a profile connecting the main gas emission sites in the southern Apennines. The graph shows that the R/Ra val-

TABLE 2. CO$_2$, CH$_4$, H$_2$ AND HE ISOTOPIC DATA OF MAIN SURFACE GAS MANIFESTATIONS FROM THE SOUTHERN APENNINES

ID	X (WGS84-UTM33E)	Y (WGS84-UTM33N)	Site	Municipality	R/Ra	^{4}He/^{20}Ne	δ^{13}C-CO$_2$ (‰, VPDB)	δ^{13}C CH$_4$ (‰, VPDB)	δ^{2}H CH$_4$ (‰VSMOW)	Mantle ^{3}He (%)	He (ppmv)	CO$_2$ (%, v/v)
1	429582	4589118	Ciorlano	Ciorlano	0.89	133.2	2.95	−29.30	−131.00	14.17	33.30	92.00
2	433158	4581775	Ailano	Ailano	0.99	153.3	1.30	−29.10	−142.00	15.76	52.12	99.40
3	404046	4554867	Sineussiane	Mondragone	1.06*	N.D.	−0.67	−25.6[†]	−136[†]	16.88	2*	98.27*
4	431765	4584378	Lete	Pratella	0.88[§]	N.D.	0.96[§]	N.D.	N.D.	14.01	94[§]	98.9[§]
5	460465	4563503	Terme Telese	Telese	1.76[#]	56[§]	−1.9[#]	N.D.	N.D.	28.03	13[#]	98.4[#]
6	521267	4503605	Terme Rosapepe	Contursi	N.D.	N.D.	0.9[§]	−30.1[†]	−135[†]	N.D.	N.D.	N.D.
7	521241	4504375	Terme Capasso	Contursi	1.35[§]	28[§]	0.68[§]	N.D.	N.D.	21.50	5[§]	94.4[§]
8	512340	4535746	Mefite Ansanto	Rocca San Felice	2.84**	239[§]	0.43[§]	−27.9[†]	−139[†]	45.22	9**	98.4**
9	518866	4506127	San Sisto	Oliveto Citra	1.33**	94[§]	0.8**	−26.6*	N.D.	21.18	17.8**	97.23*
10	571311	4528310	Maschito	Maschito	4.61**	916[§]	−1.4**	−32.5[†]	−163[†]	73.41	50**	97.01**
11	548116	4533056	Vulture Eudria	Rionero in Vulture	6.28**	11.2[§]	−3.2**	N.D.	N.D.	100.00	0.5**	99.4**

Note: Helium isotopic ratio ^{3}He/^{4}He expressed in terms of R/Ra, where R is the ratio of ^{3}H/^{4}He in the samples corrected for atmospheric (air-saturated water) contributions, compared to the ^{3}He/^{4}He in the atmosphere, Ra (1.39 10^{-6}, Craig et al., 1978). Stable C and H isotopic ratios are referred to Vienna Peedee belemnite (VPDB) and Vienna standard mean ocean water (VSMOW). He is expressed in ppmv (parts per million volume); CO$_2$ is expressed in %, v/v (volume per volume). N.D.—no data.
*Minissale (2004).
[†]Tassi et al. (2012).
[§]Minissale et al. (2016).
[#]Italiano et al. (2000).
**Caracausi et al. (2013).

ues of the Ciorlano and Ailano samples have a mantle contribution of ~15%. The increase of the mantle contribution extending southward to Mt. Vulture (considered to be the end-member) and the decrease further southward may suggest there is a gradual deepening of magma intrusions away from the volcanic center. For example, the anomalous heat flux (up to 80 mW m^{-2}) at Mefite d'Ansanto highlighted in Figure 15 can be explained by the emplacement of intrusive magmatic bodies along the main tectonic structures, which allows the rise of the mantle-derived volatiles toward the surface with CO$_2$ having the role of a carrier gas (Caracausi et al., 2013; Improta et al., 2014). Regarding heat flow, the role of aquifers in masking the real convective heat flow (i.e., associated with deep fluid discharge) of the southern Apennines should be considered, which is about five times higher than the estimated conductive heat flow of the region (40–50 mW m^{-2}; Della Vedova et al., 2001).

GeoModel

From the Tyrrhenian to Adriatic side of the mountain belt in peninsular Italy, a progressive increase in the amount of fluids emitted at the surface sourced from the upper crust has been envisaged by some researchers, which has generally been interpreted as the result of a transition from the Tyrrhenian back-arc province in the west to the chain–foredeep domain characterized by a thick continental crust in the east (e.g., Tassi et al., 2012, 2013; Caracausi and Paternoster, 2015). Some authors have presented a model based on the interaction between the crust and mantle, where the subducted portion of the Apulian Platform is pushed eastwards by the asthenospheric mantle (Doglioni, 1991;

Italiano et al., 2004). According to this model, the asthenospheric wedge would rise toward the surface in the footwall of the main normal fault related to backarc extension. Following a similar mechanism, decarbonation is envisaged to trigger CO$_2$ production within the Apulian Platform carbonates brought at depth by subduction (Doglioni, 1991). Other researchers (Chiodini et al., 2004, 2010; Improta et al., 2014; Peccerillo and Frezzotti, 2015) have considered the interaction of carbonate-rich fluids from the Apulian Platform and the rising material from the mantle and conclude that the fluids accumulated below the Apulian Platform and fed the carbonate reservoir of the buried Apulian Platform itself. If true, the thickness of the crust along the axial zone of the Apennines would be higher and the mantle wedge would be located more to the west with respect to the previous model. The presence of mafic rocks encountered by several deep wells (Improta et al., 2014) supports this second hypothesis.

The distribution of isotopic values in Figure 11 shows that the only two emission sites (Mefite d'Ansanto and Maschito) with a strong

mantle helium contribution are aligned with the Mt. Vulture volcano to the east. The resulting lineament marks the presence of a lithospheric discontinuity across the chain as already hypothesized by other authors (e.g., D'Orazio et al., 2007), rather than a west to east transition from dominantly mantle to crust-derived fluids as was suggested by the models discussed above. Furthermore, geochemical data both from this study and the literature support the hypothesis that CO$_2$ is primarily generated by the heating of the Apulian Platform carbonates and associated decarbonation, while CH$_4$ has a dry thermogenic origin. We cannot exclude the contribution of deep magmatic CO$_2$ associated with mantle melts intruded into the crust (Improta et al., 2014) and/or seismically related friction of either carbonate and/or basement rocks (Colletti et al., 2008; Famin et al., 2008; Sulem and Famin, 2009; Chiodini et al., 2011; De Paola et al., 2011; Caracausi et al., 2013). However, the dominant role of thermometamorphic and thermogenic processes for the generation of CO$_2$ and CH$_4$, respectively, appears to be in response to the emplacement
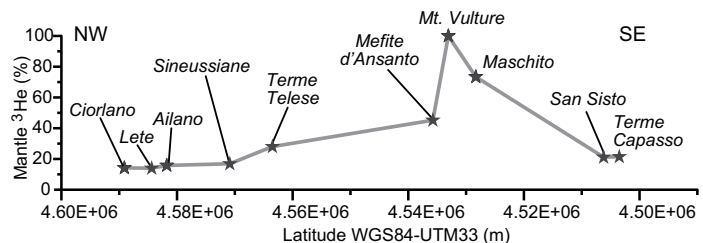

Figure 16. NW-SE profile of the mantle ^{3}He contribution (%) calculated for the R/Ra values of the data listed in Table 2 (profile trace in Fig. 15).

of magmatic sills within and at the base of the Apulian Platform. If this applies to the study area, then the exceptionally intense gas emission in the Ailano–Ciorlano area may be related to emplacement of the magmatic bodies identified by Nunziata and Gerecitano (2012) underneath the Apulian Platform carbonates, which could have led to a strong generation of CO_2 by decarbonation in recent (Quaternary) times, as is inferred from the occurrence of volcanism to the west of Matese Ridge (Fig. 1) during the Middle Pleistocene.

In the northern Apennines, the CO_2 surface flux anomaly characterizing the western part of the Italian peninsula rapidly disappears close to the active extensional front to the east. In this area, two deep wells encountered CO_2 pressures of ~98 and 67 MPa (i.e., ~0.8 of lithostatic pressure) at depths of 4750 and 3700 m b.s.l., respectively (Miller et al., 2004, and references therein). The seal for the deep fluids is represented in this area by Upper Triassic evaporites (Collettini et al., 2008). This area of limited CO_2 flux at the surface and high CO_2 fluid overpressure at depth corresponds closely to the area of active extension and seismicity (Collettini et al., 2008; Chiodini et al., 2011; Caracausi et al., 2013). In contrast, the CO_2 flux anomaly at the surface in the southern Apennines is persistent along the entire axial zone of the mountain chain where active extension and seismicity are concentrated, with both distributed soil gas emissions and vigorous gas vents following the same trend. Therefore, the role played by Upper Triassic evaporites at the base of the sedimentary cover appears to be minor in the southern Apennines, where upward migration of CO_2 into gas caps located at the top of the Apulian Platform carbonates (Inversi et al., 2013) and/or CO_2 flux to the surface are widespread. In the southern Apennines, a top seal overlies the Apulian Platform carbonate reservoirs that consists of a clay-rich mélange zone occurring at the base of the allochthonous units. However, the thickness of the mélange zone is extremely variable, reaching its maximum (~1.5 km) in the Val d'Agri area to the south (Mazzoli et al., 2001; Fig. 1B), decreasing northward to several hundreds of meters in the Irpinia area (Ascione et al., 2013) and eventually becoming extremely thin or even absent in the Matese area (Butler et al., 2004). The great thickness of the incompetent mélange zone results in an effective decoupling between deep seismogenic faults and shallow active fault segments both in the Val d'Agri (Candela et al., 2015) and in the Irpinia (Ascione et al., 2013) areas. The lack of interaction between shallow faults and the deep fluid reservoir in the Val d'Agri area is also confirmed by the very low salinity of fluid inclusions sampled from exposed fault zones, which appear to not be in direct communication with deep fault segments (Cello et al., 2001). Where the mélange zone is very thin or absent, as in the Mt. Forcuso and Matese Ridge areas (Butler et al., 2004), active fault strands at the surface are probably not decoupled from deep ones. This allows efficient pathways to be established for the rise of both crustal and mantle CO_2 and other gases toward the surface, eventually resulting in vigorous gas emissions in these areas.

Overall, the data from the Matese Ridge study suggest there is a correlation between the distribution of non-volcanic gas emissions and faults observed at the surface. The degassing process in the Matese Ridge area is primarily controlled by the major SMF crustal fault, which is several km in length and has produced Quaternary offsets on the order of at least several hundred meters. However, strong gas emissions also occur along small, active fault strands (Figs. 12, 13, and 14). These gas-bearing faults are localized in the densely fractured Pratella block and surroundings located at the western termination of the SMF, particularly in the zone interposed between the major Aquae Juliae and SMF fault zones. Such evidence suggests that in the Matese Ridge area, as has been also shown elsewhere (e.g., Fu et al., 2005; Ciotoli et al., 2007, 2014; Annunziatellis et al., 2008), degassing is preferentially localized within zones characterized by intense fracturing, which typically occurs at either terminations of active fault zones or between large, overstepping active faults zones.

CONCLUDING REMARKS

The results of our work in the southern sector of Matese Ridge in southern Italy provide new insights into the relationship between fluids (migration and shallow distribution of main leak points, i.e., gas vents) and the geometry, orientation and activity of faults. In the study area, a high flux of CO_2 is concentrated along fault strands interpreted to be active based on the detailed tectonic geomorphology analyses carried out in this study. We measured a CO_2 concentration in the soil and a CO_2 flux (preliminarily estimated to be ~500 t d^{-1}) that are among the highest non-volcanic gas emissions measured on Earth, as well as large amounts of He (up to 52 ppm). Such a high density of gas vents characterized by a high magnitude of CO_2 flux may have interesting implications for the global quantification of geogenic greenhouse gases and estimates of global climate change.

The isotope composition of C in CO_2 and CH_4 indicates that there is a dominant crustal signature, suggesting the crust and not the mantle is the main source for these gases. In particular, the buried carbonates belonging to the Apulian Platform domain are the most likely source of CO_2 produced by thermo-metamorphism. However, the percentage of mantle helium calculated for the R/Ra ratios suggests that part of the CO_2 may have a mantle source, since mantle derived intrusive bodies, reported in the borehole stratigraphic logs, may be responsible for thermo-metamorphic processes in the Apulian Platform carbonates at depth.

Based on the results obtained in this study, integrated with available regional information, it may be envisaged that the anomalously high gas emissions measured in the Ailano–Ciorlano study area result from a combination of different factors, including: (*i*) intense CO_2 generation from magmatic bodies causing decarbonation of the country rock; (*ii*) a very thin or absent clay-rich mélange zone that acts elsewhere in the southern Apennines as a top seal overlying the Apulian Platform carbonate reservoirs; and (*iii*) the occurrence of a dense network of active fault segments located at the western tip of a major crustal fault zone (i.e., the South Matese fault). The fundamental role played by the local fracture network on controlling degassing at the surface is shown by the alignment of gas vents along active fault strands and particularly by their clustering in relay ramp zones between overstepping fault segments.

REFERENCES CITED

Alessio, G., Godano, C., and Gorini, A., 1990, A low magnitude seismic sequence near Isernia (Molise, Central Italy) in January 1986: Pure and Applied Geophysics, v. 134, no. 2, p. 243–260, https://doi.org/10.1007/BF00877000.

Amato, V., Aucelli, P.P.C., Bellucci Sessa, E., Cesarano, M., Incontri, P., Pappone, G., Valente, E., and Vilardo, G., 2017, Multidisciplinary approach for fault detection: Integration of PS-InSAR, geomorphological, stratigraphic and structural data in the Venafro intermontane basin (Central-Southern Apennines, Italy): Geomorphology, v. 283, p. 80–101, https://doi.org/10.1016/j.geomorph.2017.01.027.

Amoroso, O., Ascione, A., Mazzoli, S., Virieux, J., and Zollo, A., 2014, Seismic imaging of a fluid storage in the actively extending Apennine mountain belt, southern Italy: Geophysical Research Letters, v. 41, p. 3802–3809, https://doi.org/10.1002/2014GL060070.

Amoroso, O., Russo, G., De Landro, G., Zollo, A., Garambois, S., Mazzoli, S., Parente, M., and Virieux, J., 2017, From velocity and attenuation tomography to rock physical modeling: Inferences on fluid-driven earthquake processes at the Irpinia fault system in southern Italy: Geophysical Research Letters, v. 44, p. 6752–6760, https://doi.org/10.1002/2016GL072346.

Annunziatellis, A., Beaubien, S.E., Bigi, S., Ciotoli, G., Coltella, M., and Lombardi, S., 2008, Gas migration along fault systems and through the vadose zone in the Latera caldera (central Italy): Implications for CO$_2$ geological storage: International Journal of Greenhouse Gas Control, v. 2, p. 353–372, https://doi.org/10.1016/j.ijggc.2008.02.003.

Ascione, A., and Cinque, A., 1999, Tectonics and erosion in the long term relief history of the Southern Apennines (Italy): Zeitschrift fur Geomorphologie N.F., Supplementbande, v. 118, p. 1–16.

Ascione, A., Ciarcia, S., Di Donato, V., Mazzoli, S., and Vitale, S., 2012, The Pliocene-Quaternary wedge-top basins of southern Italy: An expression of propagating lateral slab tear beneath the Apennines: Basin Research, v. 24, p. 456–474, https://doi.org/10.1111/j.1365-2117.2011.00534.x.

Ascione, A., Mazzoli, S., Petrosino, P., and Valente, E., 2013, A decoupled kinematic model for active normal faults: Insights from the 1980, MS = 6.9 Irpinia earthquake, southern Italy: Geological Society of America Bulletin, v. 125, p. 1239–1259, https://doi.org/10.1130/B30814.1.

Ascione, A., Iannace, A., Imbriale, P., Santangelo, N., and Santo, A., 2014, Tufa and travertines of southern Italy: Deep-seated, fault-related CO$_2$ as the key control in precipitation: Terra Nova, v. 26, p. 1–13, https://doi.org/10.1111/ter.12059.

Attal, M., Cowie, P.A., Whittaker, A.C., Hobley, D., Tucker, G.E., and Roberts, G.P., 2011, Testing fluvial erosion models using the transient response of bedrock rivers to tectonic forcing in the Apennines, Italy: Journal of Geophysical Research, v. 116, F02005, https://doi.org/10.1029/2010JF001875.

Aucelli, P.P.C., Cesarano, M., Di Paola, G., Filocamo, F., and Rosskopf, C.M., 2013, Geomorphological map of the central sector of the Matese Mountains (Southern Italy): An example of complex landscape evolution in a Mediterranean mountain environment: Journal of Maps, v. 9, no. 4, p. 604–616, https://doi.org/10.1080/17445647.2013.840054.

Beaubien, S.E., Ciotoli, G., Coombs, P., Dictor, M.C., Krüger, M., Lombardi, S., Pearce, J.M., and West, J.M., 2008, The impact of a naturally occurring CO$_2$ gas vent on the shallow ecosystem and soil chemistry of a Mediterranean pasture (Latera, Italy): International Journal of Greenhouse Gas Control, v. 2, no. 3, p. 373–387, https://doi.org/10.1016/j.ijggc.2008.03.005.

Beaubien, S.E., Ruggiero, L., Annunziatellis, A., Bigi, S., Ciotoli, G., Deiana, P., Graziani, S., Lombardi, S., and Tartarello, M.C., 2015, The importance of baseline surveys of near-surface gas geochemistry for CCS monitoring, as shown from onshore case studies in northern and southern Europe: Oil Gas Science Technology—Rev. IFP Energies nouvelles, v. 70, p. 615–633, https://doi.org/10.2516/ogst/2014009.

Bigi, S., Beaubien, S.E., Ciotoli, G., D'Ambrogi, C., Doglioni, C., Ferrante, V., Lombardi, S., Milli, S., Orlando, L., Ruggiero, L., Tartarello, M.C., and Sacco, P., 2014, Mantle-derived CO2 migration along active faults within an extensional basin margin (Fiumicino, Rome, Italy): Tectonophysics, v. 637, p. 137–149, https://doi.org/10.1016/j.tecto.2014.10.001.

Boschi, E., Guidoboni, E., Ferrari, G., Valensise, G., and Gasperini, P., 1997, Catalogue of strong Italian earthquakes, 461 B.C. to 1990: Bologna, Italy, ING-SGA, 644 p. and CD-ROM.

Brauer, K., Geissler, W.H., Kampf, H., Niedermann, S., and Rman, N., 2016, Helium and carbon isotope signatures of gas exhalations in the westernmost part of the Pannonian Basin (SE Austria/NE Slovenia): Evidence for active lithospheric mantle degassing: Chemical Geology, v. 422, p. 60–70, https://doi.org/10.1016/j.chemgeo.2015.12.016.

Brocchini, D., Principe, C., Castradori, D., Laurenzi, M.A., and Gorla, L., 2001, Quaternary evolution of the southern sector of the Campanian Plain and early Somma-Vesuvius activity: Insights from the Trecase 1 well: Mineralogy and Petrology, v. 73, no. 1–3, p. 67–91, https://doi.org/10.1007/s007100170011.

Bull, W.B., 2008, Tectonic Geomorphology of Mountains: A New Approach to Paleoseismology: Oxford, UK, Wiley-Blackwell Publishing, 328 p.

Burton, M.R., Sawyer, G.M., and Granieri, D., 2013, Deep carbon emissions from volcanoes: Reviews in Mineralogy and Geochemistry, v. 75, no. 1, p. 323–354, https://doi.org/10.2138/rmg.2013.75.11.

Buscher, J.T., Ascione, A., and Valente, E., 2017, Decoding the role of tectonics, incision and lithology on drainage divide migration in the Mt. Alpi region, southern Apennines, Italy: Geomorphology, v. 276, p. 37–50, https://doi.org/10.1016/j.geomorph.2016.10.003.

Butler, R.W.H., Corrado, S., Mazzoli, S., Donatis, M.D., Di Bucci, D., Naso, G., Scrocca, D., Nicolai, C., and Zucconi, V., 2000, Time and space variability of «thin-skinned» and «thick-skinned» thrust tectonics in the Apennines (Italy): Rendiconti Fisici dell': Accademia dei Lincei, v. 11, p. 5–39, https://doi.org/10.1007/BF02904594.

Butler, R.W.H., Mazzoli, S., Corrado, S., Donatis, M.D., Di Bucci, D., Gambini, R., Naso, G., Nicolai, C., Scrocca, D., Shiner, P., and Zucconi, V., 2004, Applying Thick-skinned Tectonic Models to the Apennine Thrust Belt of Italy—Limitations and Implications, *in* McClay, K.R., ed., Thrust Tectonics and Hydrocarbon System: American Association of Petroleum Geologists Memoir, v. 82, p. 647–667.

Caiazzo, C., Ascione, A., and Cinque, A., 2006, Late Tertiary-Quaternary tectonics of the Southern Apennines (Italy): New evidences from the Tyrrhenian slope: Tectonophysics, v. 421, p. 23–51, https://doi.org/10.1016/j.tecto.2006.04.011.

Calabrò, R.A., Corrado, S., Di Bucci, D., Robustini, P., and Tornaghi, M., 2003, Thin-skinned vs. thick-skinned tectonics in the Matese Massif, Central–Southern Apennines (Italy): Tectonophysics, v. 377, p. 269–297, https://doi.org/10.1016/j.tecto.2003.09.010.

Camarda, M., Guerrieri, S., and Valenza, M., 2006, CO$_2$ flux measurements in volcanic areas using the dynamic concentration method: Influence of soil permeability: Journal of Geophysical Research, v. 111, B05202, https://doi.org/10.1029/2005JB003898.

Candela, S., Mazzoli, S., Megna, A., and Santini, S., 2015, Finite element modelling of stress field perturbations and interseismic crustal deformation in the Val d'Agri region, southern Apennines, Italy: Tectonophysics, v. 657, p. 245–259, https://doi.org/10.1016/j.tecto.2015.07.011.

Caracausi, A., and Paternoster, M., 2015, Radiogenic helium degassing and rock fracturing: A case study of the southern Apennines active tectonic region: Journal of Geophysical Research. Solid Earth, v. 120, p. 2200–2211, https://doi.org/10.1002/2014JB011462.

Caracausi, A., Martelli, M., Nuccio, P.M., Paternoster, M., and Stuart, F.M., 2013, Active degassing of mantle-derived fluid: A geochemical study along the Vulture line, southern Apennines (Italy): Journal of Volcanology and Geothermal Research, v. 253, p. 65–74, https://doi.org/10.1016/j.jvolgeores.2012.12.005.

Caramanna, G., Ciotoli, G., and Nisio, S., 2008, A review of natural sinkhole phenomena in Italian plain areas: Natural Hazards, v. 45, no. 2, p. 145–172, https://doi.org/10.1007/s11069-007-9165-7.

Carapezza, M.L., and Granieri, D., 2004, CO$_2$ soil flux at Vulcano (Italy): Comparison between active and passive methods: Applied Geochemistry, v. 19, p. 73–88, https://doi.org/10.1016/S0883-2927(03)00111-2.

Cello, G., and Mazzoli, S., 1998, Apennine Tectonics in Southern Italy: A review: Journal of Geodynamics, v. 27, p. 191–211, https://doi.org/10.1016/S0264-3707(97)00072-0.

Cello, G., Guerra, I., Tortorici, L., Turco, E., and Scarpa, R., 1982, Geometry of the neotectonic stress field in southern Italy: Geological and seismological evidence: Journal of Structural Geology, v. 4, p. 385–393, https://doi.org/10.1016/0191-8141(82)90030-X.

Cello, G., Gambini, R., Mazzoli, S., Read, A., Tondi, E., and Zucconi, V., 2000, Fault zone characteristics and scaling properties of the Val d'Agri Fault system (southern Apennines, Italy): Journal of Geodynamics, v. 29, p. 293–307, https://doi.org/10.1016/S0264-3707(99)00043-5.

Cello, G., Invernizzi, C., Mazzoli, S., and Tondi, E., 2001, Fault properties and fluid flow patterns from Quaternary faults in the Apennines, Italy: Tectonophysics, v. 336, p. 63–78, https://doi.org/10.1016/S0040-1951(01)00094-4.

Chiarabba, C., and Chiodini, G., 2013, Continental delamination and mantle dynamics drive topography, extension and fluid discharge in the Apennines: Geology, v. 41, p. 715–718, https://doi.org/10.1130/G33992.1.

Chiarabba, C., Jovane, L., and Di Stefano, R., 2005, A new view of Italian seismicity using 20 years of instrumental recordings: Tectonophysics, v. 395, p. 251–268, https://doi.org/10.1016/j.tecto.2004.09.013.

Chiodini, G., and Frondini, F., 2001, Carbon dioxide degassing from the Albani Hills volcanic region, Central Italy: Chemical Geology, v. 177, no. 1, p. 67–83, https://doi.org/10.1016/S0009-2541(00)00382-X.

Chiodini, G., Frondini, F., Kerrick, D.M., Rogie, J., Parello, F., Peruzzi, L., and Zanzari, A.R., 1999, Quantification of deep CO$_2$ fluxes from Central Italy. Examples of carbon balance for regional aquifers and of soil diffuse degassing: Chemical Geology, v. 159, p. 205–222, https://doi.org/10.1016/S0009-2541(99)00030-3.

Chiodini, G., Frondini, F., Cardellini, C., Parello, F., and Peruzzi, L., 2000, Rate of diffuse carbon dioxide Earth degassing estimated from carbon balance of regional aquifers: The case of central Apennine, Italy: Journal of Geophysical Research, v. 105, no. B4, p. 8423–8434, https://doi.org/10.1029/1999JB900355.

Chiodini, G., Cardellini, C., Amato, A., Boschi, E., Caliro, S., Frondini, F., and Ventura, G., 2004, Carbon dioxide Earth degassing and seismogenesis in central and southern Italy: Geophysical Research Letters, v. 31, L07615, https://doi.org/10.1029/2004GL019480.

Chiodini, G., Granieri, D., Avino, R., Caliro, S., Costa, A., Minopoli, C., and Vilardo, G., 2010, Non-volcanic CO$_2$ Earth degassing: Case of Mefite d'Ansanto (southern Apennines), Italy: Geophysical Research Letters, v. 37, https://doi.org/10.1029/2010GL042858.

Chiodini, G., Caliro, S., Cardellini, C., Frondini, F., Inguaggiato, S., and Matteucci, F., 2011, Geochemical evidence for and characterization of CO$_2$ rich gas sources in the epicentral area of the Abruzzo 2009 earthquakes: Earth and Planetary Science Letters, v. 304, p. 389–398, https://doi.org/10.1016/j.epsl.2011.02.016.

Chiodini, G., Cardellini, C., Caliro, S., Chiarabba, C., and Frondini, F., 2013, Advective heat transport associated with regional Earth degassing in central Apennine (Italy): Earth and Planetary Science Letters, v. 373, p. 65–74, https://doi.org/10.1016/j.epsl.2013.04.009.

Ciarcia, S., Mazzoli, S., Vitale, S., and Zattin, M., 2012, On the tectonic evolution of the Ligurian accretionary complex in Southern Italy: Geological Society of America Bulletin, v. 124, p. 463–483, https://doi.org/10.1130/B30437.1.

Cinque, A., Ascione, A., and Caiazzo, C., 2000, Distribuzione spazio-temporale e caratterizzazione della fagliazione quaternaria in Appennino meridionale, *in* Galadini, F., Meletti, C., Rebez, A., eds., Le Ricerche del GNDT nel Campo della Pericolosità Sismica: CNR-GNDT, Roma, Italy, p. 107–136.

Ciotoli, G., Lombardi, S., and Annunziatellis, A., 2007, Geostatistical analysis of soil gas data in a high seismic intermontane basin: Fucino Plain, central Italy: Journal of Geophysical Research, v. 112, no. B05407, https://doi.org/10.1029/2005JB004044.

Ciotoli, G., Bigi, S., Tartarello, C., Sacco, P., Lombardi, S., Ascione, A., and Mazzoli, S., 2014, Soil gas distribution in the main coseismic surface rupture zone of the 1980, M$_S$ = 6.9, Irpinia earthquake (southern Italy): Journal of Geophysical Research. Solid Earth, v. 119, p. 2440–2461, https://doi.org/10.1002/2013JB010508.

Ciotoli, G., Etiope, G., Marra, F., Florindo, F., Giraudi, C., and Ruggiero, L., 2016, Tiber delta CO$_2$-CH$_4$ degassing: A possible hybrid, tectonically active sediment-hosted geothermal system near Rome: Journal of

Geophysical Research. Solid Earth, v. 121, p. 48–69, https://doi.org/10.1002/2015JB012557.

Collettini, C., Cardellini, C., Chiodini, G., De, P., Holdsworth, R.E., and Smith, S.A.F., 2008, Fault weakening due to CO$_2$ degassing in the Northern Apennines: Short- and long-term processes: Geological Society, London, Special Publications, v. 299, p. 175–194, https://doi.org/10.1144/SP299.11.

Corniello, A., and Russo, D., 1990, La piana del medio corso del F. Volturno (Campania) Idrogeologia e vulnerabilità all'inquinamento delle falde: Atti 1° Convegno Nazionale Protezione e Gestione delle Acque Sotterranee, p. 131–148.

Corniello, A., Ducci, D., and Guarino, P.M., 1999, The western part of the Matese carbonatic massif and Venafro plain: Hydrogeology and hydrogeochemistry: Bollettino della Società Geologica Italiana, v. 118, p. 523–535.

Craig, H., and Lupton, J.E., 1976, Primordial neon, helium and hydrogen in oceanic basalts: Earth and Planetary Science Letters, v. 31, p. 369–385, https://doi.org/10.1016/0012-821X(76)90118-7.

Craig, H., Lupton, J.E., and Horibe, Y., 1978, A mantle component in Circum-Pacific volcanic glasses: Hakone, the Marianas, and Mt. Lassen, *in* Alexander, E.C., and Ozima, M., eds., Terrestrial Rare Gases: Tokyo, Japan, Japan Scientific Society Press, 242 p., https://doi.org/10.1007/978-94-010-9828-1_1.

Day, J.M.D., Barry, P.H., Hilton, D.R., Burgess, R., Pearson, D.G., and Taylor, A.T., 2015, The helium flux from continents and ubiquity of low ^{3}He/^{4}He recycled crust and lithosphere: Geochimica et Cosmochimica Acta, v. 153, p. 116–133, https://doi.org/10.1016/j.gca.2015.01.008.

De Astis, G., Kempton, P.D., Peccerillo, A., and Wu, T.W., 2006, Trace element and isotopic variations from Mt. Vulture to Campanian volcanoes: Constraints for slab detachment and mantle inflow beneath southern Italy: Contributions to Mineralogy and Petrology, v. 151, no. 3, p. 331–351, https://doi.org/10.1007/s00410-006-0062-y.

Della Vedova, B., Mongelli, F., Pellis, G., and Zito, G., 1991, Campo regionale del flusso di calore nel Tirreno: Atti X Convegno GNGTS, p. 817–825.

Della Vedova, B., Bellani, S., Pellis, G., and Squarci, P., 2001, Deep temperatures and surface heat flow distribution, *in* Vai, G.B., and Martini, I.P., eds., Anatomy of an Orogen: The Apennines and Adjacent Mediterranean Basins: Dordrecht, The Netherlands, Springer, p. 65–76, https://doi.org/10.1007/978-94-015-9829-3_7.

De Paola, N.D., Hirose, T., Mitchell, T., Toro, G.D., Viti, C., and Shimamoto, T., 2011, Fault lubrication and earthquake propagation in thermally unstable rocks: Geology, v. 39, p. 35–38, https://doi.org/10.1130/G31398.1.

De Rita, D., Giordano, G., and Milli, S., 1998, Forestepping-backstepping stacking pattern of volcaniclastic successions: Roccamonfina volcano (Italy): Journal of Volcanology and Geothermal Research, v. 80, p. 155–178, https://doi.org/10.1016/S0377-0273(97)00069-3.

De Vivo, B., Rolandi, G., Gans, P.B., Calvert, A., Bohrson, W.A., Spera, F.J., and Belkin, H.E., 2001, New constraints on the pyroclastic eruptive history of the Campanian volcanic plain (Italy): Mineralogy and Petrology, v. 73, p. 47–65, https://doi.org/10.1007/s007010170010.

Di Bucci, D., Massa, B., Tornaghi, M., and Zuppetta, A., 2005, Structural setting of the 1688 Sannio earthquake epicentral area (Southern Italy) from surface and subsurface data: Journal of Geodynamics, v. 40, no. 2, p. 294–315, https://doi.org/10.1016/j.jog.2005.07.008.

Di Girolamo, P., Melluso, L., and Morra, V., 1991, Magmatic activity northeast of Roccamonfina volcano (southern Italy)—petrology, geochemistry and relationships with Campanian volcanics: Neues Jahrbuch für Mineralogie, Abhandlungen, v. 163, no. 2–3, p. 271–289.

DISS Working Group, 2015, Database of Individual Seismogenic Sources (DISS), Version 3.2.0: A compilation of potential sources for earthquakes larger than M 5.5 in Italy and surrounding areas. http://diss.rm.ingv.it/diss/, © INGV 2015 (Istituto Nazionale di Geofisica e Vul-
canologia) All rights reserved, https://doi.org/10.6092/INGV.IT-DISS3.2.0.

d'Italia, S.G., 1966, Foglio 172 Caserta della Carta Geologica d'Italia in scala 1:100.000: Roma, Italy, Servizio Geologico d'Italia, http://sgi.isprambiente.it/geoportal/catalog/sgilink/map100k.page (accessed June 2017).

Doglioni, C., 1991, A proposal for the kinematic modelling of W-dipping subductions - possible applications to the Tyrrhenian-Apennines system: Terra Nova, v. 3, p. 423–434, https://doi.org/10.1111/j.1365-3121.1991.tb00172.x.

D'Orazio, M., Innocenti, F., Tonarini, S., and Doglioni, C., 2007, Carbonatites in a subduction system: The Pleistocene alvikites from Mt. Vulture (southern Italy): Lithos, v. 98, no. 1, p. 313–334, https://doi.org/10.1016/j.lithos.2007.05.004.

Esposito, E., Luongo, G., Marturano, A., and Porfido, S., 1987, Il terremoto di S. Anna del 26 luglio 1805: Memorie della Societa Geologica Italiana, v. 37, p. 171–191.

Etiope, G., 2015, Natural Gas Seepage: The Earth's Hydrocarbon Degassing: Springer, 199 p., https://doi.org/10.1007/978-3-319-14601-0.

Etiope, G., and Sherwood Lollar, B., 2013, Abiotic methane on Earth: Reviews of Geophysics, v. 51, https://doi.org/10.1002/rog.20011.

Etiope, G., Baciu, C.L., and Schoell, M., 2011, Extreme methane deuterium, nitrogen and helium enrichment in natural gas from the Homorod seep (Romania): Chemical Geology, v. 280, p. 89–96, https://doi.org/10.1016/j.chemgeo.2010.10.019.

Famin, V., Nakashima, S., Boullier, A.M., Fujimoto, K., and Hirono, T., 2008, Earthquakes produce carbon dioxide in crustal faults: Earth and Planetary Science Letters, v. 265, p. 487–497, https://doi.org/10.1016/j.epsl.2007.10.041.

Ferranti, L., Milano, G., Burrato, P., Palano, M., and Cannavò, F., 2015, The seismogenic structure of the 2013–2014 Matese seismic sequence, Southern Italy: Implication for the geometry of the Apennines active extensional belt: Geophysical Journal International, v. 201, p. 823–837, https://doi.org/10.1093/gji/ggv053.

Filzmoser, P., Garrett, R.G., and Reimann, C., 2005, Multivariate outlier detection in exploration geochemistry: Computers & Geosciences, v. 31, p. 579–587, https://doi.org/10.1016/j.cageo.2004.11.013.

Fracassi, U., and Valensise, G., 2007, Unveiling the sources of the catastrophic 1456 multiple earthquake: Hints to an unexplored tectonic mechanism in southern Italy: Bulletin of the Seismological Society of America, v. 97, no. 3, p. 725–748, https://doi.org/10.1785/0120050250.

Frepoli, A., Maggi, C., Cimini, G.B., Marchetti, A., and Chiappini, M., 2011, Seismotectonic of Southern Apennines from recent passive seismic experiments: Journal of Geodynamics, v. 51, p. 110–124, https://doi.org/10.1016/j.jog.2010.02.007.

Frezzotti, M.L., Peccerillo, A., and Panza, G., 2009, Carbonate metasomatism and CO$_2$ lithosphere–asthenosphere degassing beneath the western Mediterranean: An integrated model arising from petrological and geophysical data: Chemical Geology, v. 262, no. 1, p. 108–120, https://doi.org/10.1016/j.chemgeo.2009.02.015.

Fu, C.C., Yang, T.F., Walia, V., and Cheng, C.-H., 2005, Reconnaissance of soil gas composition over the buried fault and fracture zone in southern Taiwan: Geochemical Journal, v. 39, p. 427–439, https://doi.org/10.2343/geochemj.39.427.

Galli, P., and Galadini, F., 2003, Disruptive earthquakes revealed by faulted archaeological relics in Samnium (Molise, southern Italy): Geophysical Research Letters, v. 30, no. 5, https://doi.org/10.1029/2002GL016456.

Galli, P., and Naso, J.A., 2009, Unmasking the 1349 earthquake source (southern Italy): paleoseismological and archaeoseismological indications from the Aquae Iuliae fault: Journal of Structural Geology, v. 31, p. 128–149, https://doi.org/10.1016/j.jsg.2008.09.007.

Galli, P., Giaccio, B., Messina, P., Peronace, E., Amato, V., Naso, J.A., Nomade, S., Pereira, A., Piscitelli, S., Bellanova, J., Billi, A., Blamart, D., Galderisi, A., Giocoli, A., Stabile, T., and Thil, F., 2017, Middle to Late Pleistocene activity of the northern Matese fault
system (southern Apennines, Italy): Tectonophysics, v. 699, p. 61–81, https://doi.org/10.1016/j.tecto.2017.01.007.

Gambardella, B., Cardellini, C., Chiodini, G., Frondini, F., Marini, L., Ottonello, G., and Zuccolini, M.V., 2004, Fluxes of deep CO$_2$ in the volcanic areas of central-southern Italy: Journal of Volcanology and Geothermal Research, v. 136, no. 1, p. 31–52, https://doi.org/10.1016/j.jvolgeores.2004.03.018.

Gasperini, P., Bernardini, F., Valensise, G., and Boschi, E., 1999, Defining seismogenic sources from historical earthquake felt reports: Bulletin of the Seismological Society of America, v. 89, p. 94–110.

Gautheron, C., Moreira, M., and Allègre, C., 2005, He, Ne and Ar composition of the European lithospheric mantle: Chemical Geology, v. 217, p. 97–112, https://doi.org/10.1016/j.chemgeo.2004.12.009.

Gianmanco, S., Sims, K.W.W., and Neri, M., 2007, Measurements of ^{220}Rn and ^{222}Rn and CO$_2$ emissions in soil and fumarole gases on Mt. Etna volcano (Italy): Implications for gas transport and shallow ground fractures: Geochemistry, Geophysics, Geosystems, v. 8, no. 10, p. 1–14, https://doi.org/10.1029/2007GC001644.

Googas, 2006, Results of INGV-DPCV5 project: The catalogue of Italian gas emissions: http://googas.ov.ingv.it (accessed June 2017).

Hack, J.T., 1957, Studies of longitudinal stream profile in Virginia and Maryland: U.S. Geological Survey Professional Paper, v. 194, no. B, p. 45–97.

Hippolyte, J.C., Angelier, J., and Roure, F., 1994, A major geodynamic change revealed by Quaternary stress patterns in the Southern Apennines (Italy): Tectonophysics, v. 230, p. 199–210, https://doi.org/10.1016/0040-1951(94)90135-X.

Holland, P.W., and Emerson, D.E., 1990, The global helium-4 content of near-surface atmospheric air, *in* Geochemistry of Gaseous Elements and Compounds: Athens, Greece, Theophrastus Publications, S.A., p. 97–113.

Improta, L., and Corciulo, M., 2006, Controlled source nonlinear tomography: A powerful tool to constrain tectonic models of the Southern Apennines orogenic wedge, Italy: Geology, v. 34, p. 941–944, https://doi.org/10.1130/G22676A.1.

Improta, L., De Gori, P., and Chiarabba, C., 2014, New insights into crustal structure, Cenozoic magmatism, CO$_2$ degassing, and seismogenesis in the southern Apennines and Irpinia region from local earthquake tomography: Journal of Geophysical Research. Solid Earth, v. 119, no. 11, p. 8283–8311, https://doi.org/10.1002/2013JB010890.

Inversi, B., Scrocca, D., Montegrossi, G., Livani, M., Petracchini, L., Brandano, M., Brilli, M., Giustini, F., Recanati, R., and Gola, G., 2013, 3D geological modelling of a fractured carbonate reservoir for the study of medium enthalpy geothermal resource in the Southern Apennines (Campania Region, Italy): Pisa, Italy, Proceedings European Geothermal Congress.

Italiano, F., Martelli, M., Martinelli, G., and Nuccio, P.M., 2000, Geochemical evidence of melt intrusions along lithospheric faults of the Southern Apennines, Italy: Geodynamic and seismogenic implications: Journal of Geophysical Research, v. 105, no. B6, p. 13569–13578, https://doi.org/10.1029/2000JB900047.

Italiano, F., Martinelli, G., and Rizzo, A., 2004, Geochemical evidence of seismogenic-induced anomalies in the dissolved gases of thermal waters: A case study of Umbria (Central Apennines, Italy) both during and after the 1997–1998 seismic swarm: Geochemistry, Geophysics, Geosystems, v. 5, https://doi.org/10.1029/2004GC000720.

Italiano, F., Martinelli, G., and Plescia, P., 2008, CO$_2$ Degassing over Seismic Areas: The Role of Mechanochemical Production at the Study Case of Central Apennines: Pure and Applied Geophysics, v. 165, p. 75–94, https://doi.org/10.1007/s00024-007-0291-7.

Italiano, F., Bonfanti, P., Pizzino, L., and Quattrocchi, F., 2010, Geochemistry of fluids discharged over the seismic area of the Southern Apennines (Calabria region, Southern Italy): Implications for fluid–fault relationships: Applied Geochemistry, v. 25, p. 540–554, https://doi.org/10.1016/j.apgeochem.2010.01.011.

Kirby, E., and Whipple, K.X., 2001, Quantifying differential rock-uplift rates via stream profile analysis: Geology, v. 29, p. 415–418, https://doi.org/10.1130/0091-7613 (2001)029<0415:QDRURV>2.0.CO;2.

Lambiase, S., and Ruggiero, A., 1980, La forra del Torano (Matese Centrale): Un caso di convergenza fra morfogenesi carsica e fluviale: Atti della Società Toscana di Scienze Naturali–Memorie, p. 171–192.

Locati, M., Camassi, R., and Stucchi, M., 2011, DBMI11, the 2011 version of the Italian Macroseismic Database: Milano, Italy, http://emidius.mi.ingv.it/DBMI11 (accessed December 2017).

Luhr, J.F., and Giannetti, B., 1987, The brown leucitic tuff of Roccamonfina Volcano (Roman region, Italy): Contributions to Mineralogy and Petrology, v. 95, no. 4, p. 420–436, https://doi.org/10.1007/BF00402203.

Lupton, J.E., and Craig, H., 1975, Excess ^{3}He in oceanic basalts: Evidence for terrestrial primordial helium: Earth and Planetary Science Letters, v. 26, no. 2, p. 133–139, https://doi.org/10.1016/0012-821X(75)90080-1.

Macchiavelli, C., Mazzoli, S., Megna, A., Saggese, F., Santini, S., and Vitale, S., 2012, Applying the Multiple Inverse Method to the analysis of earthquake focal mechanism data: New insights into the active stress field of Italy and surrounding regions: Tectonophysics, v. 580, p. 124–149, https://doi.org/10.1016/j.tecto .2012.09.007.

Maggi, C., Frepoli, A., Cimini, G.B., Console, R., and Chiappini, R., 2009, Recent seismicity and crustal stress field in the Lucanian Apennines and surrounding areas (Southern Italy): Seismotectonic implications: Tectonophysics, v. 463, p. 130–144, https://doi.org/10 .1016/j.tecto.2008.09.032.

Magro, G., and Pennisi, M., 1991, Noble gases and nitrogen: Mixing and temporal evolution in the fumarolic fluids of Vulcano, Italy: Journal of Volcanology and Geothermal Research, v. 47, no. 3–4, p. 237–247, https://doi .org/10.1016/0377-0273(91)90003-I.

Martelli, M., Nuccio, P.M., Stuart, F.M., Burgess, R., Ellam, R.M., and Italiano, F., 2004, Helium–strontium isotope constraints on mantle evolution beneath the Roman Comagmatic Province, Italy: Earth and Planetary Science Letters, v. 224, p. 295–308, https://doi.org/10 .1016/j.epsl.2004.05.025.

Mazzoli, S., and Helman, M., 1994, Neogene patterns of relative plate motion for Africa-Europe: Some implications for recent central Mediterranean tectonics: Geologische Rundschau, v. 83, p. 464–468.

Mazzoli, S., Barkham, S., Cello, G., Gambini, R., Mattioni, L., Shiner, P., and Tondi, E., 2001, Reconstruction of continental margin architecture deformed by the contraction of the Lagonegro basin, Southern Apennines, Italy: Journal of the Geological Society, v. 158, p. 309–320, https://doi.org/10.1144/jgs.158.2.309.

Mazzoli, S., D'Errico, M., Aldega, L., Corrado, S., Invernizzi, C., Shiner, P., and Zattin, M., 2008, Tectonic burial and "young" (<10 Ma) exhumation in the southern Apennines fold-and-thrust belt (Italy): Geology, v. 36, p. 243–246, https://doi.org/10.1130/G24344A.1.

Mazzoli, S., Szaniawski, R., Mittiga, F., Ascione, A., and Capalbo, A., 2012, Tectonic evolution of Pliocene-Pleistocene wedge-top basins of the Southern Apennines: New constraints from magnetic fabric analysis: Canadian Journal of Earth Sciences, v. 49, p. 492–509, https://doi.org/10.1139/e11-067.

Mazzoli, S., Ascione, A., Buscher, J.T., Pignalosa, A., Valente, E., and Zattin, M., 2014, Low-angle normal faulting and focused exhumation associated with late Pliocene change in tectonic style in the southern Apennines (Italy): Tectonics, v. 33, p. 1802–1818, https://doi .org/10.1002/2014TC003608.

Michetti, A.M., Blumetti, A.M., Esposito, E., Ferreli, L., Guerrieri, L., Porfido, S., Serva, L., and Vittori, E., 2000, Earthquake Ground Effects and Seismic Hazard Assessment in Italy examples from the Matese and Irpinia areas, Southern Apennines, *in* Active Fault Research for the New Millennium: Hokudan, Japan, Proceedings of the Hokudan Symposium and School on Active Faulting, p. 279–284.

Milano, G., Di Giovambattista, R., and Alessio, G., 1999, Earthquakes swarms in the Southern Apennines chain (Italy): The 1997 seismic sequence in the Sannio–

Matese mountains: Tectonophysics, v. 306, p. 57–78, https://doi.org/10.1016/S0040-1951(99)00040-2.

Milano, G., Ventura, G., and Di Giovambattista, R., 2002, Seismic evidence of longitudinal extension in the Southern Apennines chain (Italy): The 1997–1998 Sannio–Matese seismic sequence: Geophysical Research Letters, v. 29, no. 20, https://doi.org/10.1029 /2002GL015188.

Milano, G., Di Giovambattista, R., and Ventura, G., 2005, The 2001 seismic activity near Isernia (Italy): Implications for the seismotectonics of the Central–Southern Apennines: Tectonophysics, v. 401, no. 3, p. 167–178, https://doi.org/10.1016/j.tecto.2005.03.010.

Milano, G., Di Giovambattista, R., and Ventura, G., 2006, Seismicity and stress field in the Sannio-Matese area: Annals of Geophysics Supplement, v. 49, no. 1, p. 347–356.

Miller, S.A., Collettini, C., Chiaraluce, L., Cocco, M., Barchi, M., and Kaus, B.J., 2004, Aftershocks driven by a high-pressure CO_2 source at depth: Nature, v. 427, p. 724–727, https://doi.org/10.1038/nature02251.

Minissale, A., 2004, Origin, transport and discharge of CO_2 in central Italy: Earth-Science Reviews, v. 66, p. 89–141, https://doi.org/10.1016/j.earscirev.2003.09.001.

Minissale, A., Donato, A., Procesi, M., Gianmanco, S., and Pizzino, L., 2016, Dati e Carte geochimiche del Mezzogiorno d'Italia, *in* Manzella, A., ed., Progetto Atlante Geotermico del Mezzogiorno, CNR per il Mezzogiorno, CNR-IGG, ISBN: 9788879580298, 57 p.

Morley, C.K., and Wonganan, N., 2006, Subsidence in the super-deep Pattani and Malay basins of Southeast Asia: A coupled model incorporating lower-crustal flow in response to post-rift sediment loading: Basin Research, v. 18, p. 51–84, https://doi.org/10.1111/j.1365-2117 .2006.00285.x.

Mörner, N.A., and Etiope, G., 2002, Carbon degassing from the lithosphere: Global and Planetary Change, v. 33, no. 1, p. 185–203, https://doi.org/10.1016/S0921-8181 (02)00070-X.

Nunziata, C., and Gerecitano, F., 2012, VS crustal models of the Roccamonfina volcano and relationships with Neapolitan volcanoes (southern Italy): International Journal of Earth Sciences, v. 101, no. 5, p. 1371–1383, https://doi.org/10.1007/s00531-011-0722-7.

Paonita, A., Caracausi, A., Martelli, M., and Rizzo, A.L., 2012, Temporal variations of helium isotopes in volcanic gases quantify pre-eruptive refill and pressurization in magma reservoirs: The Mount Etna case: Geology, v. 44, no. 7, p. 499–502, https://doi.org/10 .1130/G37807.1.

Paris, S., and Sevink, J., 1983, Late Wurmian to early Holocene lake deposits and pyroclastics in the middle Volturno basin (Caserta province, Italy): Geologica Romana, v. 22, p. 207–210.

Patacca, E., and Scandone, P., 2001, Late thrust propagation and sedimentary response in the thrust-belt—foredeep system of the Southern Apennines (Pliocene-Pleistocene), *in* Vai, G.B., Martini, I.P., eds., Anatomy of an Orogen: The Apennines and Adjacent Mediterranean Basins: Dordrecht, The Netherlands, Springer, p. 401–440, https://doi.org/10.1007/978-94-015-9829-3_23.

Peccerillo, A., and Frezzotti, M.L., 2015, Magmatism, mantle evolution and geodynamics at the converging plate margins of Italy: Journal of the Geological Society, v. 172, p. 407–427, https://doi.org/10.1144 /jgs2014-085.

Pondrelli, S., Salimbeni, S., Ekström, G., Morelli, A., Gasperini, P., and Vannucci, G., 2006, The Italian CMT dataset from 1977 to the present: Physics of the Earth and Planetary Interiors, v. 159, no. 3–4, p. 286–303, https://doi.org/10.1016/j.pepi.2006.07.008.

Porfido, S., Esposito, E., Vittori, E., Tranfaglia, G., Guerrieri, L., and Pece, R., 2007, Seismically induced ground effects of the 1805, 1930 and 1980 earthquakes in the Southern Apennines (Italy): Bollettino della Società Geologica Italiana, v. 126, no. 2, p. 333–346.

Principe, C., 2006, La Geologia del Monte Vulture: Regione Basilicata and Consiglio Nazionale delle Ricerche, 217 p.

Reimann, C., Filzmoser, P., and Garrett, R.G., 2005, Background and threshold: Critical comparison of

methods of determination: The Science of the Total Environment, v. 346, p. 1–16, https://doi.org/10.1016/j .scitotenv.2004.11.023.

Rizzo, A., Caracausi, A., Favara, R., Martelli, M., Paonita, A., Paternoster, M., Nuccio, P.M., and Rosciglione, A., 2006, New insights into magma dynamics during last two eruptions of Mount Etna as inferred by geochemical monitoring from 2002 to 2005: Geochemistry, Geophysics, Geosystems, v. 7, no. 6, Q06008, https://doi .org/10.1029/2005GC001175.

Rolandi, G., Bellucci, F., Heizler, M.T., Belkin, H.E., and De Vivo, B., 2003, Tectonic controls on the genesis of ignimbrites from the Campanian Volcanic Zone, southern Italy: Mineralogy and Petrology, v. 79, p. 3–31, https://doi.org/10.1007/s00710-003-0014-4.

Romanak, K.D., Bennet, P., Yang, C., and Hovorka, S.D., 2012, Process-based approach to CO_2 leakage detection by vadose zone gas monitoring at geologic CO_2 storage sites: Geophysical Research Letters, v. 39, p. L15405, https://doi.org/10.1029/2012GL052426.

Rouchon, V., Gillot, P.Y., Quidelleur, X., Chiesa, S., and Floris, B., 2008, Temporal evolution of the Roccamonfina volcanic complex (Pleistocene), Central Italy: Journal of Volcanology and Geothermal Research, v. 177, no. 2, p. 500–514, https://doi.org/10.1016/j.jvolgeores .2008.07.016.

Rovida, A., Locati, M., Camassi, R., Lolli, B., and Gasperini, P., 2016, CPTI15, the 2015 version of the Parametric Catalogue of Italian Earthquakes: Istituto Nazionale di Geofisica e Vulcanologia, http://doi.org/10.6092/INGV .IT-CPTI15 (accessed December 2017).

Sano, Y., and Marty, B., 1995, Origin of carbon in fumarolic gas from island arcs: Chemical Geology, Isotope Geoscience Section, v. 119, p. 265–274.

Santangelo, N., Daunis-i-Estadella, J., Di Crescenzo, G., Di Donato, V., Faillace, P.I., Martín-Fernández, J.A., Romano, P., and Scorpio, V., 2012, Topographic predictors of susceptibility to alluvial fan flooding, Southern Apennines: Earth Surface Processes and Landforms, v. 37, no. 8, p. 803–817, https://doi.org/10 .1002/esp.3197.

Santangelo, N., Romano, P., Ascione, A., and Russo Ermolli, E., 2017, Quaternary evolution of the Southern Apennines coastal plains: A review: Geologica Carpathica, v. 68, no. 1, p. 43–56, https://doi.org/10.1515/geoca -2017-0004.

Santangelo, N., and Santo, A., 1991, Endokarstic evolution of carbonate massifs in Campania (southern Italy): Geological and geomorphological implications, *in* Proceedings of the International Conference on Environmental Changes in Karst Areas: ICECKA: Italy, 15–27 September 1991: Quaderni del Dipartimento di Geografia, v. 13, p. 83–93.

Santo, A., Ascione, A., Del Prete, S., Di Crescenzo, G., and Santangelo, N., 2011, Collapse sinkholes distribution in the carbonate massifs of central and southern Apennines: Acta Carsologica, v. 40, p. 95–112.

Sartori, R., 2003, The Tyrrhenian backarc basin and subduction of the Ionian lithosphere: Episodes, v. 26, p. 217–221.

Savelli, C., and Schreider, A.A., 1991, The opening processes in the deep Tyrrhenian basins of Marsili and Vavilov, as deduced from magnetic and chronological evidence of their igneous crust: Tectonophysics, v. 190, p. 119–131, https://doi.org/10.1016/0040-1951 (91)90358-Y.

Serva, L., Esposito, E., Guerrieri, L., Porfido, S., Vittori, E., and Comerci, V., 2007, Environmental effects from five historical earthquakes in southern Apennines (Italy) and macroseismic intensity assessment: Contribution to INQUA EEE Scale Project: Quaternary International, v. 173, no. 17, p. 30–44, https://doi.org/10.1016 /j.quaint.2007.03.015.

Shiner, P., Beccacini, A., and Mazzoli, S., 2004, Thin-skinned versus thick-skinned structural models for Apulian carbonate reservoirs: Constraints from the Val d'Agri Fields, S Apennines, Italy: Marine and Petroleum Geology: Oil and Gas in Compressional Belts, v. 21, p. 805–827, https://doi.org/10.1016/j.marpetgeo .2003.11.020.

Sibson, R., 1981, A brief description of natural neighbor interpolation. Interpreting multivariate data, *in* Barnet,

V., ed., Interpreting Multivariate Data: Chichester, UK, Wiley, p. 21–36.

Sinclair, A.J., 1991, A fundamental approach to threshold estimation in exploration geochemistry: Probability plots revisited: Journal of Geochemical Exploration, v. 41, no. 1–2, p. 1–22, https://doi.org/10.1016/0375 -6742(91)90071-2.

Speranza, F., and Chiappini, M., 2002, Thick-skinned tectonics in the external Apennines, Italy: New evidence from magnetic anomaly analysis: Journal of Geophysical Research, v. 107, https://doi.org/10.1029 /2000JB000027.

Steckler, M.S., Agostinetti, N.P., Wilson, C.K., Roselli, P., Seeber, L., Amato, A., and Lerner-Lam, A., 2008, Crustal structure in the Southern Apennines from teleseismic receiver functions: Geology, v. 36, p. 155–158, https://doi.org/10.1130/G24065A.1.

Sulem, J., and Famin, V., 2009, Thermal decomposition of carbonates in fault zones: Slip-weakening and temperature-limiting effects: Journal of Geophysical Research. Solid Earth, v. 114, no. B3, https://doi.org/10 .1029/2008JB006004.

Tassi, F., Capecchiacci, F., Cabassi, J., Calabrese, S., Vaselli, O., Rouwet, D., Pecoraino, G., and Chiodini, G., 2012, Geogenic and atmospheric sources for volatile organic compounds in fumarolic emissions from Mt. Etna and Vulcano Island (Sicily, Italy): Journal of Geophysical Research. Atmospheres, v. 117, no. D17, https://doi .org/10.1029/2012JD017642.

Tassi, F., Nisi, B., Cardellini, C., Capecchiacci, F., Donnini, M., Vaselli, O., Avino, R., and Chiodini, G., 2013, Diffuse soil emission of hydrothermal gases (CO_2, CH_4, and C_6H_6) at Solfatara crater (Campi Flegrei, southern Italy): Applied Geochemistry, v. 35, p. 142–153, https://doi.org/10.1016/j.apgeochem.2013.03.020.

Tedesco, D., 1997, Systematic variations in the ^{3}He/^{4}He ratio and carbon of fumarolic fluids from active vol-

canic areas in Italy: Evidence for radiogenic ^{4}He and crustal carbon addition by the subducting African plate?: Earth and Planetary Science Letters, v. 151, p. 255–269, https://doi.org/10.1016/S0012-821X (97)81852-3.

Turco, E., Macchiavelli, C., Mazzoli, S., Schettino, A., and Pierantoni, P.P., 2012, Kinematic evolution of Alpine Corsica in the framework of Mediterranean mountain belts: Tectonophysics, v. 579, p. 193–206.

Valensise, G., and Pantosti, D., 2001, Seismogenic faulting, moment release patterns and seismic hazard along the central and southern Apennines and Calabrian Arc, *in* Vai, G.B., and Martini, I.P., eds., Anatomy of an Orogen: The Apennines and Adjacent Mediterranean Basins. Dordrecht, The Netherlands, Kluwer Academic Publishing, p. 495– 512, https://doi.org/10.1007/978 -94-015-9829-3_27.

Valente, E., Ascione, A., Ciotoli, G., Cozzolino, M., Porfido, S., and Sciarra, A., 2018, Do moderate magnitude earthquakes generate seismically induced ground effects? The case study of the Mw = 5.16, 29th December 2013 Matese earthquake (southern Apennines, Italy): International Journal of Earth Sciences, v. 107, no. 2, p. 517–537, https://doi.org/10.1007/s00531-017 -1506-5.

Vaselli, O., Nisi, B., Tassi, F., Rappuoli, D., Pancioli, V., Ucciero, S., and Giannini, L., 2011, CO_2 hazard vs touristic attraction at Mt. Amiata volcano (Italy): Acta Vulcanologica, v. 23, no. 1–2, p. 73–80.

ViDEPI Project, 2010, Ministero dello Sviluppo Economico (UNMIG): Assomineraria, http://unmig .sviluppoeconomico.gov.it/videpi/videpi.asp (accessed November 2016).

Vitale, S., Dati, F., Mazzoli, S., Ciarcia, S., Guerriero, V., and Iannace, A., 2012, Modes and timing of fracture network development in poly-deformed carbonate reservoir analogues, Mt. Chianello, southern Italy: Jour-

nal of Structural Geology, v. 37, p. 223–235, https://doi .org/10.1016/j.jsg.2012.01.005.

Vitale, S., Fedele, L., Tramparulo, F.D., Ciarcia, S., Mazzoli, S., and Novellino, A., 2013, Structural and petrological analyses of the Frido Unit (southern Italy): New insights into the early tectonic evolution of the southern Apennines–Calabrian Arc system: Lithosphere, v. 168–169, p. 219–235, https://doi.org/10.1016/j .lithos.2013.02.006.

Westaway, R., 1992, Seismic moment summation for historical earthquakes in Italy: Tectonic implications: Journal of Geophysical Research, v. 97, p. 15437–15464, https://doi.org/10.1029/92JB00946.

Whipple, K.X., Wobus, C., Kirby, E., Crosby, B., and Sheehan, D., 2007, New Tools for Quantitative Geomorphology: Extraction and Interpretation of Stream Profiles from Digital Topographic Data: Denver, Colorado, USA, Short Course presented at Geological Society of America Annual Meeting, 27–31 October 2007.

Whittaker, A.C., Cowie, P.A., Attal, M., Tucker, G.E., and Roberts, G.P., 2007, Bedrock channel adjustment to tectonic forcing: Implications for predicting river incision rates: Geology, v. 35, p. 103–106, https://doi.org /10.1130/G23106A.1.

Whittaker, A.C., Attal, M., Cowie, P.A., Tucker, G.E., and Roberts, G.P., 2008, Decoding temporal and spatial patterns of fault uplift using transient river long profiles: Geomorphology, v. 100, p. 506–526, https://doi .org/10.1016/j.geomorph.2008.01.018.